National University Rail Center - NURail
US DOT OST-R Tier 1 University Transportation Center

NURail Project ID: NURail2014-UIUC-R09

Modeling the Lateral Load Distribution for Multiple Concrete Crossties and Fastening Systems

By

Bassem Andrawes, Ph.D.
Associate Professor
Department of Civil and Environmental Engineering
University of Illinois at Urbana-Champaign
andrawes@illinois.edu

31-01-2017

Grant Number: DTRT12-G-UTC18 (Grant 1)

DISCLAIMER

Funding for this research was provided by the NURail Center, University of Illinois at Urbana - Champaign under Grant No. DTRT12-G-UTC18 of the U.S. Department of Transportation, Office of the Assistant Secretary for Research & Technology (OST-R), University Transportation Centers Program. The contents of this report reflect the views of the authors, who are responsible for the facts and the accuracy of the information presented herein. This document is disseminated under the sponsorship of the U.S. Department of Transportation's University Transportation Centers Program, in the interest of information exchange. The U.S. Government assumes no liability for the contents or use thereof.

TECHNICAL SUMMARY

Title

Modeling the Lateral Load Distribution for Multiple Concrete Crossties and Fastening Systems

Introduction

The objective of this project was to further investigate the performance of concrete crosstie and fastening system under vertical and lateral wheel load using finite element analysis, and explore possible improvement for current track design standard. The damage of fastening system is one of the most prevalent failure causes for concrete crosstie track, however the current AREMA design standard only includes evaluative tests for the fastening system, rather than a mechanistic design approach. To improve the current design approach, the vertical and lateral load path through the track structure and the component demand within the concrete crosstie and fastening system should be further investigated.

Approach and Methodology

The research work included the following tasks: 1) developing a detailed finite element model of the prestressed concrete crosstie and fastening system based on the manufacturer's design, 2) validating the component models of the rail clip and the prestressed concrete crosstie based on manufacturer's information and crosstie flexural test, 3) validating the single-crosstie-fastening-system model based on laboratory experimentation, 4) validating the multiple crosstie model based on the field experimentation conducted on instrumented track, 5) validating the multiple crosstie model based on full-scale laboratory experimentation under asymmetric loading scenarios, 6) using the validated FE model to conduct parametric studies about the failure mechanisms of the concrete crosstie and fastening system, and the effect of critical design parameters on the performance of the track structure,

Findings

Based on the model validation at different levels, it is proven that the detailed finite element model is able to capture some critical mechanisms of the track structure including the rotation of the rail, the response of the fastening system, the distribution of wheel loads and the flexure of concrete crosstie. In addition, the field validation of the finite element model and the parametric

studies provide some valuable insights on the load path and performance of the continuous track structure.

Conclusions

Based on the model validation at different levels and the parametric studies using the field-validated FE model, some conclusions can be summarized from this study:

• Under field conditions, the vertical rail seat load of the loaded rail seat varied between 25% and 62.5% of the vertical wheel load.

• In the track configuration used for field experimentation, the lateral wheel load mainly distributed among the three nearest rail seats, which is contrary to conventional wisdom.

• The elastic modulus of the fastening system insulator has little effect on the lateral load path through the fastening system.

• Compared to the COF at the rail-pad and plate-concrete interfaces, and the elastic modulus of rail pad, crosstie spacing has a very minimal impact on the performance of the fastening system under lateral wheel load.

• The COF at the rail-pad and the plate-concrete interfaces, and the elastic modulus of the rail pad significantly affect the performance of the fastening system under lateral wheel load.

Recommendations

In this study, finite element models of the concrete crosstie and fastening system were built to investigate the performance of continuous track structure under static wheel loads. However, as a large portion of the track component failures are due to impact loading, the impact analysis of the track structure is recommended to better understand the possible difference in wheel load path between static and impact loading scenarios. In addition, the longitudinal wheel load due to braking/accelerating and thermal effect is also critical to the deformation of the track structure. In future studies it is recommended to consider the combined effect of vertical, lateral, and longitudinal wheel load on the track structure as in this study only a combination of vertical and lateral wheel load is considered.

Publications

Zhe Chen, Moochul Shin, Bassem Andrawes, and John Riley Edwards (2014) "Parametric study on Damage and Load Demand of Prestressed Concrete Crosstie and Fastening Systems" Engineering Failure Analysis, Vol. 46, p. 49-61.

Zhe Chen, Moochul Shin, Sihang Wei, Bassem Andrawes, and Daniel Kuchma (2014) "Finite Element Modeling and Validation of Fastening Systems and Concrete Sleepers in North America" Journal of Rail and Rapid Transit, Vol. 228, n 6, p. 590-602

Primary Contact

Principal Investigator
Bassem Andrawes
Associate Professor
Department of Civil and Environmental Engineering
University of Illinois at Urbana-Champaign
(217)244-4178
andrawes@illinois.edu

NURail Center
217-244-4999
nurail@illinois.edu
http://www.nurailcenter.org/

On the following page you would start the text of your final report. Be sure to follow the NURail formatting guidelines.

TABLE OF CONTENTS

SECTION 1: INTRODUCTION 1
SECTION 2: FINITE ELEMENT MODEL 4
SECTION 3: PARAMETRIC STUDIES ON THE CONCRETE CROSSTIE AND FASTENING SYSTEM 18
SECTION 4: CONCLUSIONS AND RECOMMENDATIONS 44

SECTION 1: INTRODUCTION

1.1 Background

Materials including wood, reinforced concrete and polymeric composites have been used for crosstie in the railroad industry in North America, and due to historical reasons wood crosstie has been most widely used. However, many of the new mainline constructions have changed to concrete crosstie for higher material strength and longer lifespan. The advantage of concrete crosstie can be summarized in several aspects: in comparison with wood crosstie, reinforced concrete crosstie can withstand a higher wheel loading when used at the same crosstie spacing, and prestress can further improve the performance of concrete crosstie. In addition, concrete crosstie has better resistance for deterioration under severe weather conditions and therefore a longer replacement cycle could be expected. The drawback of concrete crosstie is the poor damping property that may result in material damage under high impact loading, but it could be compensated by resilient components in the fastening system. Therefore, it can be concluded that concrete crosstie has some advantages over traditional wood crosstie in satisfying the demand of high-speed rail and heavy-haul freight transportation. Figure 1.1 shows a typical design of prestressed concrete crosstie.

a) b)

Figure 1.1. a) A typical design of prestressed concrete crosstie, b) concrete crosstie used on railroad

The fastening system is fixed to the concrete crosstie to transmit loading from the rail to the concrete surface and maintain uniform track geometry. Fastening systems of various designs are used in practice and different systems consist of different components. As shown in Figure 1.2, the fastening system modeled in this study includes embedded iron shoulders, clips, nylon insulators, and a rail-seat pads system consisting of a resilient polyurethane pad for load attenuation and a nylon abrasion plate to mitigate abrasion of the concrete. The embedded shoulder provides support for other components. The clip is deformed initially and inserted into the shoulder to prevent longitudinal and lateral displacement of the rail. The insulator is placed between the clip and the rail to provide electrical isolation between the two rails to ensure the signal system is not shunted.

Figure 1.2. Layout of the fastening system in this study

1.2 Research Necessity

In the Track and Rail and Infrastructure Integrity Compliance Manual published by Federal Railroad Administration (FRA), the allowable deviation of rail head from uniform geometry is defined for different track classes (FRA 2012). "Alinement" is defined as the line uniformity in horizontal plan of each rail, and "gage" is defined as the distance between the two rails measured 15.9 mm (0.625 in) below the top surface of the rail. Both the alinement and the gage of a track section are related to the performance of the fastening system under lateral wheel load. While some pass/fail evaluative tests are defined in the AREMA Manual to ensure the quality of the fastening system, limited guideline is provided for railroad engineers to design or verify a fastening system towards the requirement a certain track class. In addition, there is an increasing demand in North America on the railroad infrastructure and its components due to ever heavier axle loads from freight trains and because of the interest to run higher-speed passengers on predominantly freight lines. The dominant design approach for concrete crosstie and fastening systems are iterative, empirical, and based on speed and traffic to determine the design load in American Railroad Engineering and Maintenance-of-way Association (AREMA)'s Recommended Practices (AREMA 2012). To ensure that freight and

passengers are transported safely and that the necessary track geometry is maintained, further investigation into the behavior and interaction of the concrete crosstie and fastening system is needed. To facilitate the transfer in railroad infrastructure from empirical design to mechanistic design, it is critical to quantify the load path through which the vertical and lateral load is transmitted from the wheel to the substructure. At the same time mechanistic models that describe the load path through the concrete crosstie and fastening system should be developed so that the methodology of mechanistic design can be practically applied.

The Rail Transportation and Engineering Center (RailTEC) at the University of Illinois at Urbana-Champaign (UIUC) conducted a survey on the international railway industry's state of practice regarding the concrete crossties and fastening systems design, performance and research needs (FRA 2013). The results from the survey highlighted the most prevalent failure causes resulting in concrete crosstie and fastening system deficiencies. The international response and domestic responses (North America) were quite different in terms of the most prevalent failure causes. In North America, the most prevalent failure cause is concrete deterioration beneath the rail, and 43% of the respondents indicated fastening system damage was associated with their operating environment. Outside of North America, fastening system damage is the most prevalent failure causes and was reported by 50% of the respondents. Besides, improper component design has drawn attention of both. Based on the result of the international survey, it can be observed that the damage and design of fastening system have become important concerns for the safety of railroad infrastructure.

1.3 Research Objectives

This study uses finite element (FE) analysis to further investigate the performance and design of concrete crosstie and fastening system with the aim of proposing improvements to the current AREMA design standard. The objectives of this research can be divided into two parts:

- Develop detailed FE models of the concrete crosstie and fastening system to accurately simulate their performance under vertical and lateral wheel load.
- Conduct comprehensive parametric study based on FE models to investigate the load path through the track superstructure and some prevalent failure mechanisms.

SECTION 2: FINITE ELEMENT MODEL

The track structure is a continuous structure system of infinite length. To accurately capture the behavior of the track superstructure (concrete crosstie and fastening system), the FE model needs to include a track structure segment of significant length. In addition, the fastening system installed on each rail seat consists of a number of components, and the modeling of interaction among fastening system components is computationally expensive. To ensure the FE model is both accurate and computationally efficient, the submodeling technique is implemented. A detailed model is built to capture the local behavior close to the application of the wheel load, and a global model is built to provide realistic boundary condition for the detailed model.

The modeling work was carried out using ABAQUS (Dassault Systemes Simulia Corp. 2011) Standard. In ABAQUS a finite element analysis is performed through definition in different modules including “part”, “property”, “assembly”, “steps”, “interaction”, “load”, “mesh”, “job”, and “visualization”. To provide a detailed description for the development of the FE model, the global and detailed model are firstly introduced, and the detailed model is used as an example for the model definitions in different modules.

2.1 Finite Element Model Configuration: Detailed Model

In order to examine the responses of the fastening system under different loading scenarios, a 3D FE model that includes one set of fastening system on a single concrete crosstie with simplified supports is developed. Figure 2.1 illustrates the layout of the fastening system in the detailed FE model. In the working environment, the wheel load can be divided into a vertical load, which is applied on the top of the railhead, and a lateral load, which is applied at edge of the railhead.

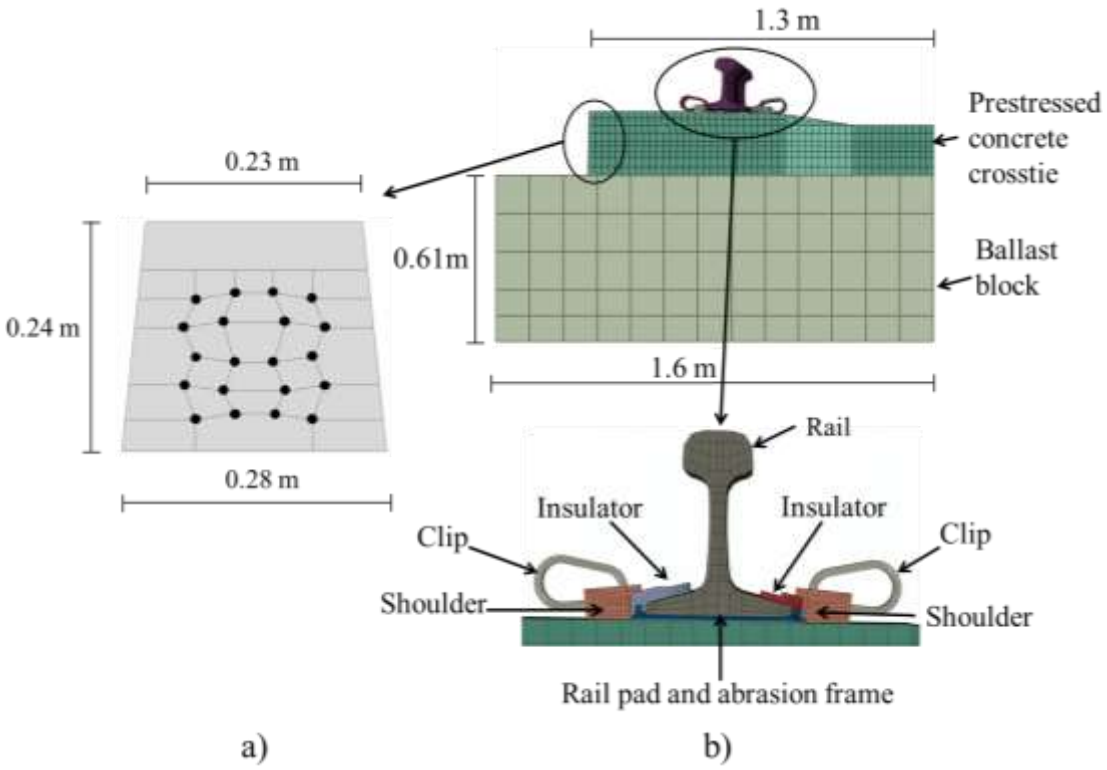

Figure 2.1. a) Configuration of the 3D concrete crosstie model and b) fastening system FE model

As shown in Figure 2.1, the model consists of one set of fastening systems as described above, and a single symmetric prestressed concrete crosstie. The design of concrete crosstie and fastening system modeled in this study is widely installed on heavy freight track in North America. The dimension of the crosstie is 2.59 m (102 in) (length) x 0.28 m (11 in) (width) x 0.24 m (9.5 in) (height) with 20 embedded prestressing strands. The section area of the prestressing strand is 22 mm^2, and the distribution of prestressing strands in the concrete crosstie is shown in Figure 2.1a.

2.2 Finite Element Model Configuration: Global Model

To simulate the behavior of continuous rail supported by multiple concrete crossties and fastening systems, a simplified global model was built to collaborate with the detailed model. The global model includes five concrete crossties at a spacing of 0.61 m (24 in) and five sets of fastening system. The number of crossties to be included in the global model was determined based on a sensitivity test that compared the response of FE models with different number of crossties and different crosstie spacing. It was shown that the effect of a single vertical and lateral wheel load on the track structure is limited to the five nearest crossties. As it was designed based on field tests where symmetric wheel loading was applied, symmetric boundary conditions were defined in the model, and a single rail with 5 symmetric concrete crossties was included, as shown in Figure 2.2. In the global model, the material property definition is the same as that in the detailed

model. In addition, the mesh and the component geometry are simplified to reduce calculation time. Instead of installing the rail clips to apply clamping force, pressure is defined on the surface of insulators to simulate the clamping force.

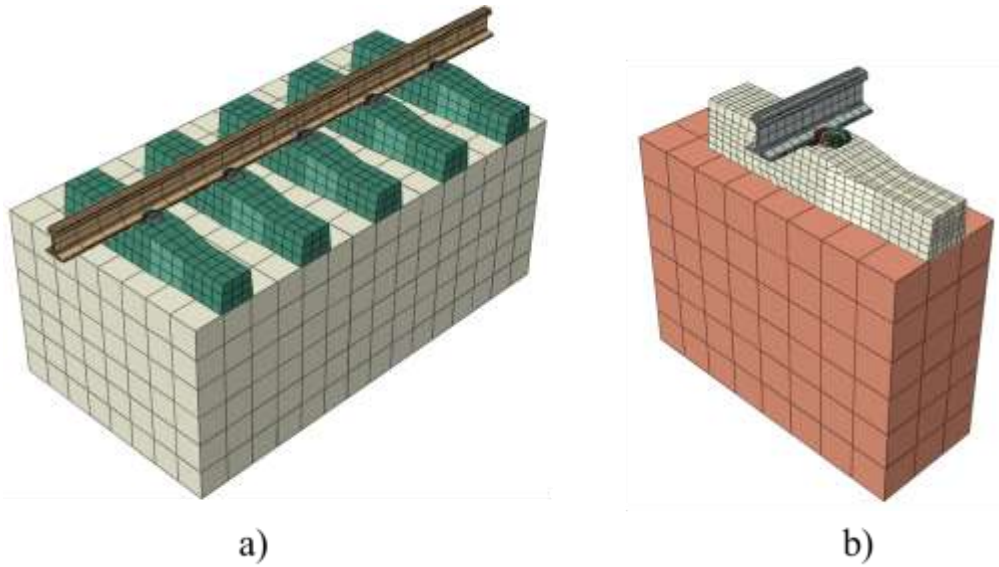

Figure 2.2 Comparison between a) the global model and b) the detailed model

To simulate a loading scenario, the global model is run first. Afterwards during the calculation of the detailed model, the displacement at the end of rail segment in the global model is introduced so that the rail segment in the detailed model behaves the same as part of the longer rail segment in the global model. In addition, as shown in Figure 2.3, the vertical and lateral load shared by adjacent concrete crossties is resisted by the displacement boundary condition at the end of the rail segment. As a result, the concrete crosstie in the detailed model behaves identically as the center crosstie in the global model, while the output accuracy is considerably increased.

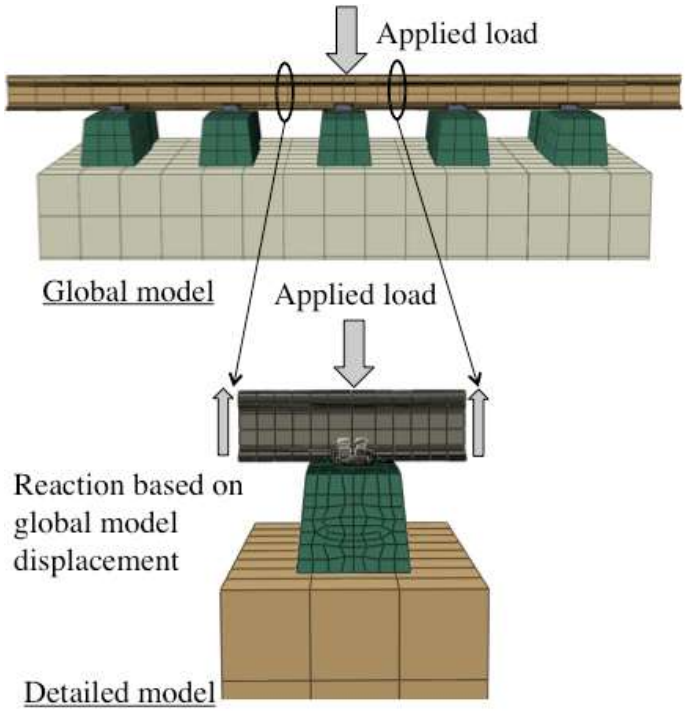

Figure 2.3 Interaction of the global and detailed models

3.3 Component Geometry and Assembly

In ABAQUS, the geometry of the component models is defined in the "part" module, and then in the "assembly" module the component models are placed into the same coordinate system to form the FE model for the analysis. The user can design the geometry of model components in ABAQUS or import existing geometry file. In this model the geometries of all the components were generated and simplified in Adobe Inventor Professional based on designs provided by the manufacturers, and some of the component models are shown in Figure 2.4. In the detailed model, a 0.61-meter (24 in) rail segment of 136 RE section is modeled at the rail seat.

In the "assembly" module, copies of the component models are introduced into the same coordinate system, and they could be rotated or translated to represent the experimental setting required by the analysis. While different copies of the same component model could be placed differently, the geometry, material property, and finite element meshing of all the copies are identical to the original component model.

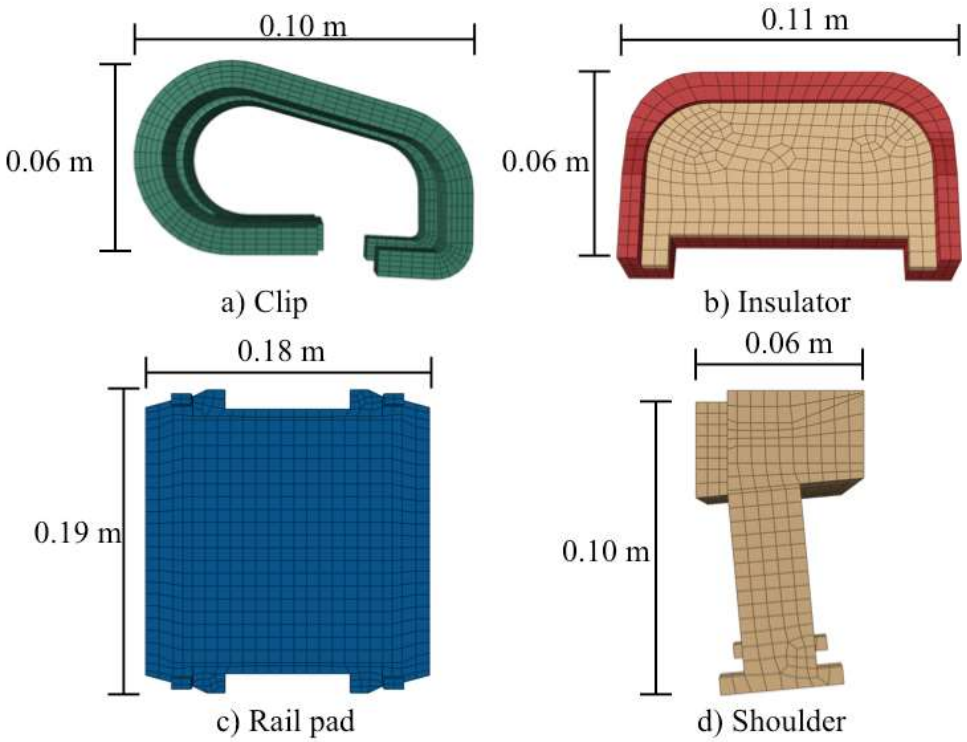

Figure 2.4 Component FE models of: a) rail clip, b) insulator, c) rail pad, and d) shoulder

2.4 Material Property

The material property of different component models are defined in the "property" module. In ABAQUS the concrete material property could be defined using the concrete smeared cracking model, or the concrete damaged plasticity model. A concrete damaged plasticity model was used in this research as it is designed for general cases in which concrete is under monotonic, cyclic, or dynamic loading with low confining pressure. Two main failure mechanisms were considered, namely concrete tensile cracking and compressive crushing. Under uniaxial tension, concrete maintain the same stiffness in the linear-elastic stage, and after the cracking stress is reached it follows a softening stress-strain relationship. Under uniaxial compression, concrete remains linear-elastic until the yielding stress is reached. In the plastic stage, the concrete is first characterized by strain hardening and then strain softening after reaching the ultimate compressive stress (see Figure 2.5). As cyclic loading was not included in current model, the two damage parameters related to unloading stiffness were not defined.

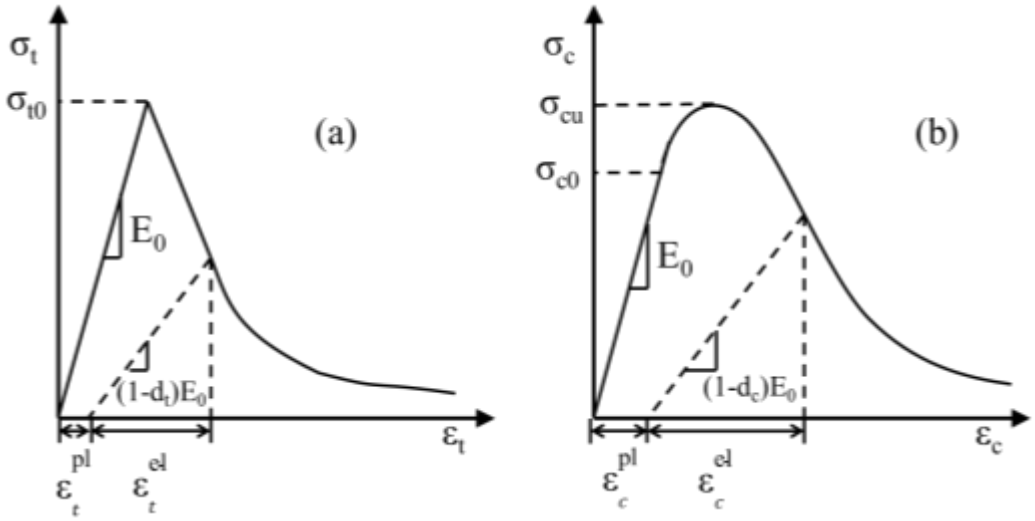

Figure 2.5 Stress-strain relationship of concrete in a) tension and b) compression

For all the fastening system components including shoulder, clip, rail pad, abrasion plate, insulator as well as the rail, a two-stage material property model was defined. In the initial stage, the material follows a linear-elastic relationship. The plastic stage consists of a strain-hardening range followed by a strain-softening range. The material property of concrete crosstie and fastening system was defined based on manufacturer's information and are shown in Table 2.1.

Table 2.1 Material property of the model components

Component	**Young's Modulus (GPa)**	**Poisson's Ratio**	**Yielding Strength (MPa)**	**Ultimate/Peak Strength (MPa)**	**Cracking Strength (MPa)**
Concrete	30.0	0.2	NA	48.3	5.5
Clip	158.6	0.29	1261.8	1393.2	
Rail	206.9	0.3	1034.3	1034.3	
Insulator	3.0	0.39	64.1	84.8	
Rail Pad	0.1	0.49	8.3	35.9	
Abrasion Plate	3.0	0.39	64.1	84.8	

Researchers have used different approaches to simulate the performance of the track substructure under wheel loads. Huang and Tutumluer (2011) used discrete element modeling to investigate the effect of fouling on the strength of ballast. The approach is

able to accurately capture the ballast performance, however the modeling process is computationally expensive. Yu et al. (2011) used the extended Druker-Prager model to define the material property of the ballast, and a layer of infinite element was defined around the ballast to simulate the effect of the subgrade. However, the process to determine the material property of the infinite element was not clearly described. As the proposed FE model focused on the performance of prestressed concrete crosstie and fastening system, a support block was introduced as the general representation of the track substructure, which consists of ballast, subballast, subgrade, etc. To capture the nonlinear vertical stiffness of the track substructure, a hyperelastic model was used to define the material property of the support block. This material model is usually used for nonlinear elastic materials with little compressibility.

2.5 Component Interaction

The interaction between different surfaces, the bond-slip behavior between concrete and reinforcement, and the interaction between embedded shoulder insert and concrete are defined in the "interaction" module. Contact pairs in ABAQUS were used to define the interactions between different components of the fastening system, and between crossties and the ballast (see Figure 3.6) (Dassault Systemes Simulia Corp. 2011). A master surface and a slave surface of different mesh densities were identified for surface-to-surface contact. Different contact properties were defined about the tangential behavior of the interfaces based on the tribological characteristics of different materials, and a coefficient of friction (COF) is assigned for each contact property. Some of the COF values were based on a series of large-scale abrasion resistance tests that were conducted at UIUC (Kernes et al. 2012), and others were determined based on empirical data (Stachowiak and Batchelor 2013; Yamaguchi 1990). The COF defined for the interactions are summarized in Table 2.2.

Table 3.2 COFs defined in the FE model

Component Name	**Frictional Interaction**	**COF Value**
Pad	Pad-frame	0.3
	Pad-rail	0.3
Abrasion Frame	Frame-concrete	0.3
Insulator	Insulator-rail	0.15
	Insulator-clip	0.15
	Insulator-shoulder	0.15

Shoulder	Shoulder-clip	0.5
Crosstie	Crosstie-ballast	0.7

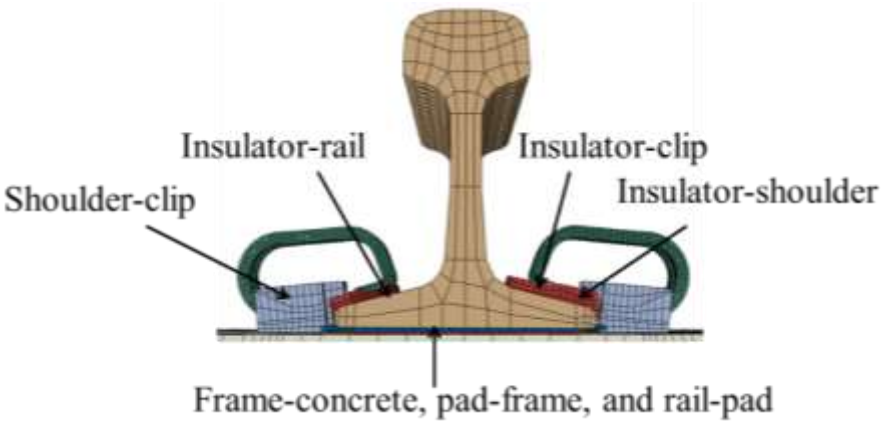

Figure 2.6 Locations of the interaction definitions

The interaction between the concrete crosstie and embedded shoulder inserts is complex as it involves multiple pairs of interacting surfaces. To simplify the mesh of concrete and to avoid numerical singularity, an "embedded region" in ABAQUS was used to model the interaction. By defining this constraint, the translational degrees of freedom on a group of elements are controlled by the response of the host elements that they are embedded in, as shown in Figure 2.7. The embedded element could be 1-D truss/beam element, 2-D membrane element, or 3-D solid element. This technique is often used to model rebar-reinforced structures. To define this constraint, the element of the concrete crosstie is picked as the host region, and the element of shoulder insert is picked as the embedded region. In this case, the nodes of the embedded element (shoulder element) are restrained by the nodes of the host element (concrete element). And with "embedded region" the bond characteristics between concrete and shoulder insert can be reasonably represented until damage occurs.

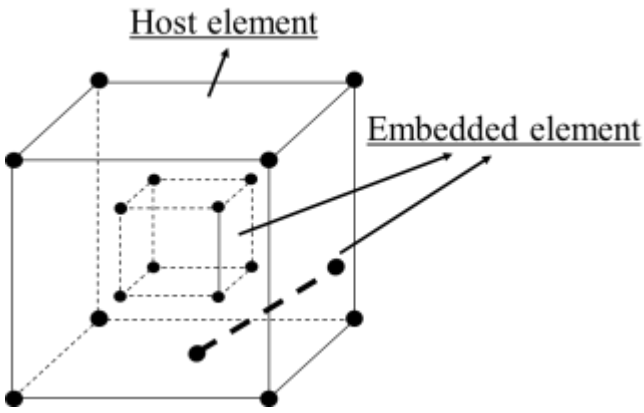

Figure 2.7 Schematics for the “embedded region” constraint

Researchers used different approaches to simulate the bond-slip behavior between concrete and reinforcement. Yu et al. (2011) used cohesive element to model the concrete-reinforcement interface. However the material property of the cohesive element is not explained in detail, and the geometry needed for cohesive element will result in some difficulty for the meshing of concrete element. The “embedded region” in ABAQUS also provides an alternative to simulate the interaction between the concrete and the reinforcement. But by using “embedded region”, it is assumed that the reinforcement is fully bonded to the concrete, and no relative sliding is allowed between them. In this study, connector elements were used to define the interaction between the concrete and prestressed wires. By using connector elements between concrete and reinforcement, realistic bond-slip behavior based on concrete pull-out test could be introduced in the FE model. The concrete was meshed in a way that element nodes along the line of the wires coincided with wire nodes, and a connector element connected the coincident concrete and wire nodes, as shown in Figure 2.8. The Cartesian connector section was assigned to the connector element, and the connector element acted as a spring based on the relative displacements of the connected nodes. Connector element with Cartesian section is able to provide connection between two nodes and allows independent linear or nonlinear force-displacement relationship in three local Cartesian directions. For simplification the bond-slip behavior was averaged over the length of reinforcement, and an elastic force-displacement relationship was defined for all the connectors. The stiffness along the direction of the wires was defined based on the pullout test results of similar materials (Holste et al. 2014). In addition, rigid connection was defined in the other two directions of connector elements.

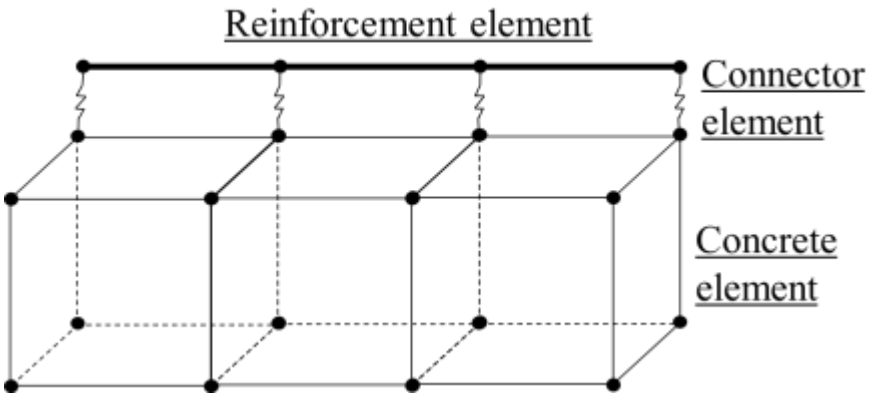

Figure 2.8 Schematics for the connection between concrete element and reinforcement element

2.6 Loading and Boundary Conditions

To define the loading scenarios for a finite element analysis in ABAQUS, analysis steps are firstly defined in the "step" module, and within each analysis step different loadings and boundary conditions are defined in the "loading" module. In each analysis step, the loadings, boundary conditions, and interactions between different components remain the same, and among different analysis steps variation could be introduced in these three aspects to simulate a loading sequence in experimentation. In ABAQUS, different analysis step types are provided for different types and focus of experimentation, including static step, dynamic step, cyclic step, etc. As the laboratory and field experimentation included in this study mainly focused on the static response of the railroad track structure, static analysis steps are used in the finite element analysis.

In the "loading" module, loadings, boundary conditions, and predefined stress field could be defined in the analysis steps to simulate a specific loading scenario. The loading could be defined in the analysis in the form of point load, pressure, body force, etc. And the magnitude of the loading could be defined as a function of step time by choosing the appropriate amplitude. In this analysis, the vertical and lateral wheel loads are defined as point load applied on the rail head, and pressure is applied on the surface of clip toe to pre-deform the rail clips before installation. Boundary conditions are defined in the analysis to provide support for the system model, or introduce predefined displacement to some model components. In this analysis, different boundary conditions are defined for the release of prestress, installation of rail clips, and the support of the substructure. By creating predefined field, an initial stress field can be assigned to the model before any loading is applied. In this analysis a uniform initial stress field is defined on the reinforcement of the concrete crosstie to simulate the stress state of the reinforcement after pre-tensioning.

In total, the model includes seven static analysis steps, and the schematics for the loading steps are shown in Figure 2.9. In the initial step a total prestress force of 623 kN (140

kips) was assigned to 20 wires based on manufacturer design, which is 80% of the wire tensile capacity, and the prestress was gradually released. The loading and boundary conditions on the clips are designed to simulate the actual installation process using manual clippers. In the first step, clips were lifted with pressure loading on the surface of the clip toes while the clip base was restrained with boundary condition. In the second step, as the rail clips were already pre-deformed in the previous step, they were inserted into shoulders with displacement boundary condition and clamping force was applied to the system with the pressure loading removed. It is proven that the performance of the rail clip is affected by both the normal and tangential force on the clip toes, and the loading and boundary condition during the installation of the clip were defined to ensure the friction between the clip and the insulator was correctly simulated.

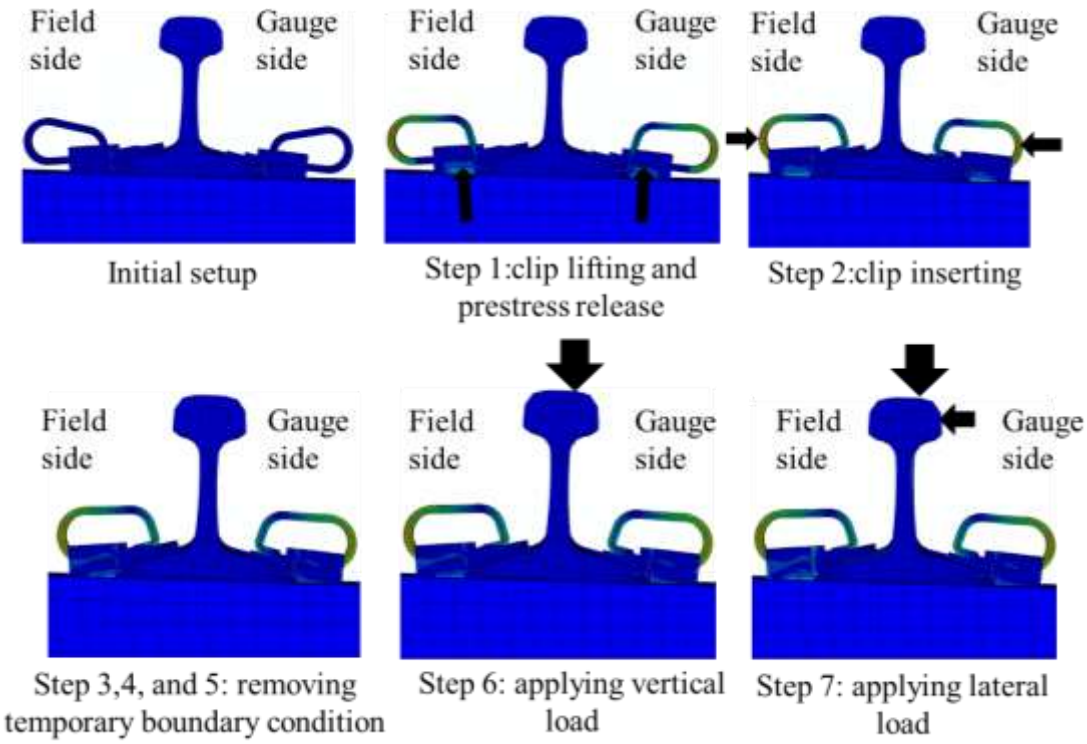

Figure 2.9 Loading sequence of the FE model

In static FE modeling, the analysis will fail to converge if the model has no stiffness for any possible degree of freedom. As a result, in the model stabilizing boundary conditions and loadings are defined in the initial steps when the interaction between component models are gradually established. In the following three steps (step 3, 4 and 5), stabilizing boundary conditions and loadings were gradually removed from the model, and at the end of the fifth step the model was ready for wheel load. At this time a vertical boundary condition was applied at the bottom of the support block to provide support for the system, and a symmetric boundary condition was applied at the centerline section of the track structure. In the sixth step, a vertical wheel load was applied as a point load and linearly increased to the maximum value. In the seventh step, while the vertical loading remained constant, the lateral wheel load was applied as a point load on the lateral

surface of the rail head and linearly increased to the target value (see Figure 2.10). The loading scenarios are discussed in detail in later sections.

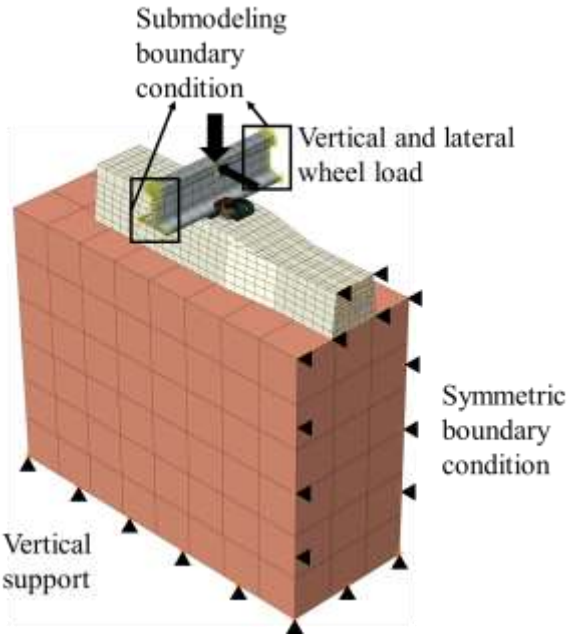

Figure 2.10 Loading scenario of the detailed FE model under vertical and lateral wheel load

3.7 Meshing

In ABAQUS, the size, shape and type of element, and the meshing techniques are defined in the "mesh" module. The user should initially define the desirable size and type of element to be used in the analysis, and then ABAQUS will be able to automatically generate component mesh based on the defined geometry, partition and meshing technique. Three types of 3-D element are provided in ABAQUS including tetrahedral element, triangular prism element, and hexahedral (or brick) element. To reduce the number of element, the rail, fastening system, concrete crosstie and supporting ballast were all modeled with eight-node brick element. This type of element has three translational degrees of freedom (DOF) at each node. The prestressing reinforcement was modeled with 1-D truss element that only had stiffness along the longitudinal direction (see Figure 2.11), as it should have minimal flexural stiffness considering its aspect ratio. Based on the result of mesh sensitivity analysis and the geometry of the components, different mesh densities were assigned to different components. For the clip, as large deformation occurred and the component response was sensitive to mesh density when applying clamping forces, dense mesh was assigned; and as the ballast only served as the general representation of the track substructure, it was coarsely meshed. The mesh densities of all the components were determined with mesh sensitivity analysis, and the mesh sensitivity of the clip is shown as an example in Figure 2.12. It can be observed that finer mesh does not significantly affect the behavior of clip, and the clip mesh with 10,292 elements was used in further studies. Figure 2.4 also shows the relative density of

mesh. Meshing techniques including “structured meshing” and “swept meshing” are used to automatically generate the finite element mesh on different component models. Structured meshing uses simple predefined mesh topologies to generate meshes, and is more appropriate for regularly shaped components (rail pad, crosstie, etc.). And swept meshing is used to mesh component models of relatively complex geometry (insulator, rail, etc.).

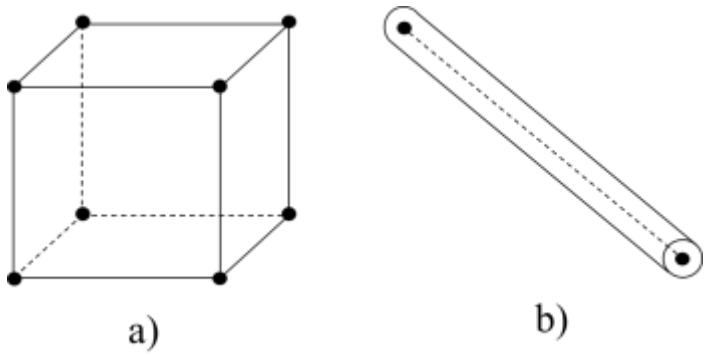

Figure 2.11 a) Eight-node brick element and b) two-node truss element used in the finite element analysis

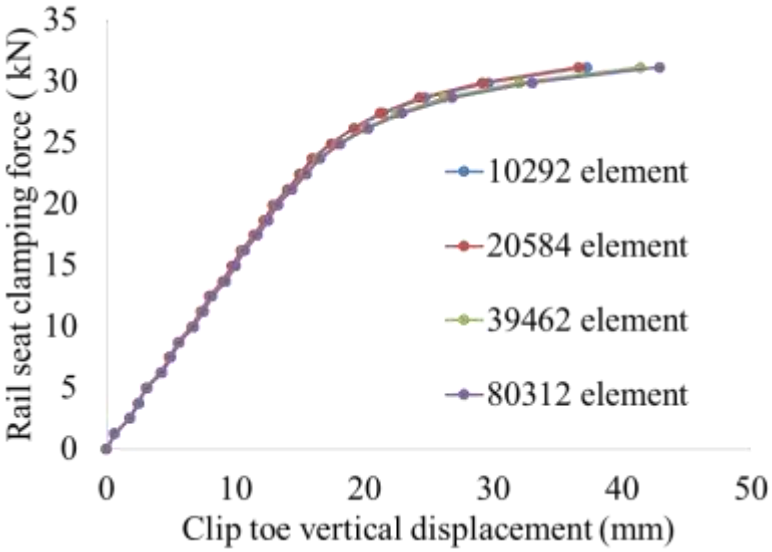

Figure 2.12 Comparison of the clamping-force displacement relationship of clip models with different mesh densities

2.8 Analysis Job and Output

Based on the definitions in all the modules mentioned, a FE model and the corresponding analysis type is established. In the "job" module of ABAQUS, a job can be defined and submitted to initiate the required FE analysis. In the process the information included in the model file (".cae" file) will be written into an input file (".inp" file), and at the end of the analysis an output database (".odb" file) will be generated, which includes all the output of a FE analysis. In this module the user is able to initiate, monitor, and terminate an analysis job. In this study, due to the large number of cases generated in the parametric analysis, all the analysis is performed using parallel execution to expedite the process.

The output database file generated in the FE analysis could be opened in "visualization" module. This module provides graphic display of finite element models and results. A contour plot of a specific analysis variable (displacement, strain, etc.) could be provided at a certain step time, and the time history of a specific quantity through the whole analysis could also be generated.

SECTION 3: PARAMETRIC STUDIES ON THE CONCRETE CROSSTIE AND FASTENING SYSTEM

The symmetric FE models are used in this chapter in two sets of parametric studies based on different experimental designs: in the first set of parametric study, the FE models are modified to investigate some critical component failure mechanisms related to the cracking of concrete crossties; in the second set of parametric study, the FE models are used to investigate the effects of some critical design parameters on the load path and the performance of the track structure.

3.1 Failure Mechanism Analysis of the Concrete Crosstie and Fastening System

3.1.1 Prestress and bond-slip behavior

As the concrete crosstie is a prestressed flexural member, and the rail seat loads are applied close to the ends of the crosstie, it is important to determine the transfer length of the prestressed concrete crosstie so that its flexural capacity could be fully utilized. The bond-slip behavior between concrete and strands is crucial to the performance of the prestressed concrete crosstie as it determines the initial stress state of concrete before any loading. To investigate the effect of the bond-slip behavior between concrete and reinforcement on the prestress state of concrete crosstie, a component model of concrete crosstie was built. The component model was the same as described above, and only one loading step was defined, which included the release of prestress. As mentioned before the bond-slip behavior was simplified and an elastic force-displacement relationship was defined for the connectors. The elastic stiffness of connectors served as the varying parameter in this parametric study. Based on some available pull-out test results in literature (Abrishami and Mitchell 1993; Du et al. 2010; Mitchell and Marzouk 2007; Rose and Russell 1997), four elastic stiffness values were chosen for this parametric study including 137,888 kN/m/m (20000 lb/in/in), 275,777 kN/m/m (40000 lb/in/in), 413,665 kN/m/m (60000 lb/in/in) and 551,553 kN/m/m (80000 lb/in/in). The four cases were generated to represent a realistic range of possible bond-slip behavior in prestressed concrete crossties.

During release of the concrete crosstie, one critical parameter is the transfer length, which is defined as the length from the end of the strand to the point where the effective stress is developed. In the field, the wheel loading is applied at the two rail-seat regions, and it would be desirable to have fully transferred prestress in the rail-seat regions. As the four cases represent the range of possible bond-slip behavior in prestressed concrete crosstie, the output of the four cases were used to evaluate the range of transfer length of existing prestressed concrete crossties. The transfer lengths of the four models are summarized in Figure 3.1. The transfer lengths were determined based on the concrete surface compressive strain in the longitudinal direction at the centroid height of prestressing strands using 95% Average Maximum Strain (AMS) method, as shown in Figure 3.1.

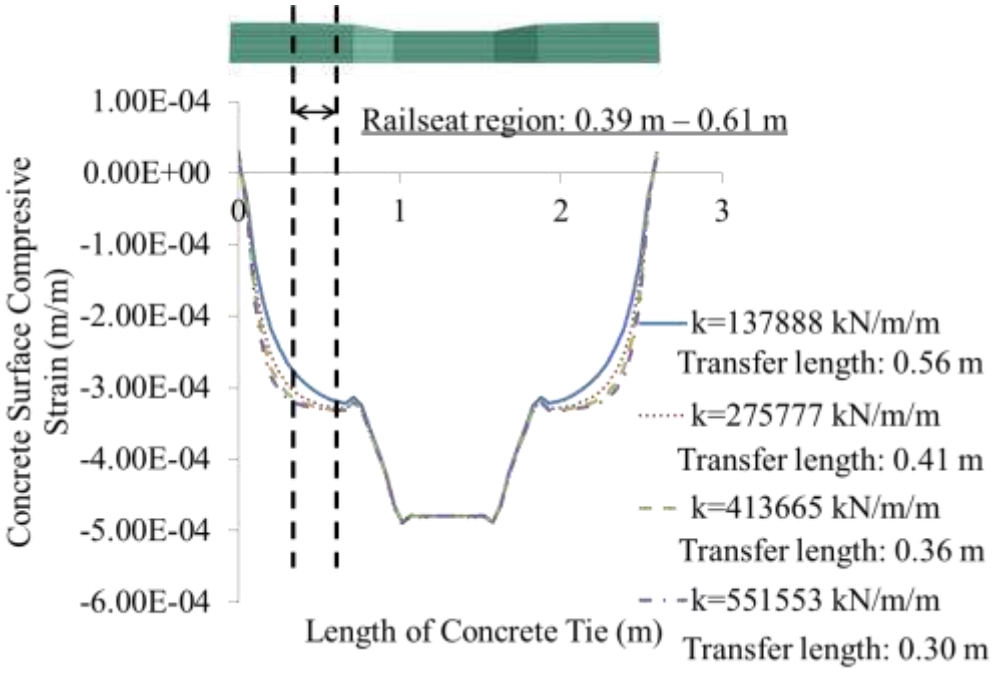

Figure 3.1 Concrete surface strain distribution along the length of concrete crosstie

Considering the end of concrete crosstie as the origin point, the distance of the rail-seat region of the concrete crosstie falls between 0.39 m (15.4 in) and 0.61 m (24 in). In 2012, Murphy presented the transfer length measurement of 220 prestressed concrete crossties. The crossties were provided by four major manufacturers of concrete crosstie in North America (Murphy 2012). In comparison, the transfer length of the cases generated in this parametric study is within the range of the laboratory measurement. In the two cases where the bond-slip stiffness was defined as 137,888 kN/m/m (20000 lb/in/in) and 275,777 kN/m/m (40000 lb/in/in), the rail-seat region was partially included in the transfer-length region; and in the other two cases where higher bond-slip stiffness was defined, the transfer length was shorter than 0.39 m (15.4 in) and the concrete prestress was fully transferred in the rail-seat region. When the elastic stiffness of connectors increased from 137,888 kN/m/m (20000 lb/in/in) to 275,777 kN/m/m (40000 lb/in/in), the transfer length reduced from 0.56 m (22 in) to 0.41 m (16 in). However, when the elastic stiffness of connectors was relatively high, further increase in the elastic stiffness only resulted in a small reduction in transfer length. In summary, the case with bond-slip stiffness of 275777 kN/m/m (40000 lb/in/in) is the threshold for desirable transfer length, and the any weaker bond between concrete and prestressing reinforcement results in insufficient prestress in the rail-seat region. The threshold can also be expressed as 16501 MPa/m (60.6 ksi/in), which is the equivalent pullout stress divided by reinforcement end slip.

3.1.2 Center binding

The cracking of concrete crosstie due to center binding has been identified as one of the critical problems that result in the failure of the concrete crosstie and fastening system

(FRA 2013). The mechanism for center binding begins as the support of ballast under the crosstie is initially concentrated at the rail-seat rather than uniformly distributed (Lutch et al. 2009). Over time as the cyclic loading of the vehicles is applied, the depression and abrasion of the ballast is most severe under the rail-seat area of the crosstie. As a result, firm support of the ballast is only provided at the center of the crosstie, and the crosstie cantilevers over its two ends. Under the new support condition, when wheel loading is applied, large negative moment exists at the midspan and results in tensile cracking at the top surface. Figure 3.2 shows an example of the tensile cracks due to center binding in concrete crossties.

Figure 3.2 Cracked concrete crosstie due to center binding

To simulate the support condition that causes center binding, the geometry of the ballast was changed according to the field observation described in references (Lutch et al. 2009). Firm support was provided at the midspan of the crosstie, and two slopes were placed close to the rail seat, which allowed a gap between the concrete crosstie and the ballast at the rail-seat area. Based on the model deflection of concrete crosstie and literatures regarding the depression of the ballast (Huang and Tutumluer 2011), four models with firm support (i.e. no gap), 1.27 mm (0.05 in) gap, 2.54 mm (0.1 in) gap, and 3.81 mm (0.15 in) gap were built and compared in terms of the concrete crosstie response. The FE model with exaggerated gaps under rail-seat regions is shown in Figure 3.3. A vertical loading of 267 kN (60 kips) was applied in increments to both rail-seats, and a lateral loading of 133.5 kN (30 kips) was applied to one rail-seat to simulate the loading scenario of curved track. The loading scenario was determined based on the load environment specified in AREMA Chapter 30 for mainline freight traffic in North America.

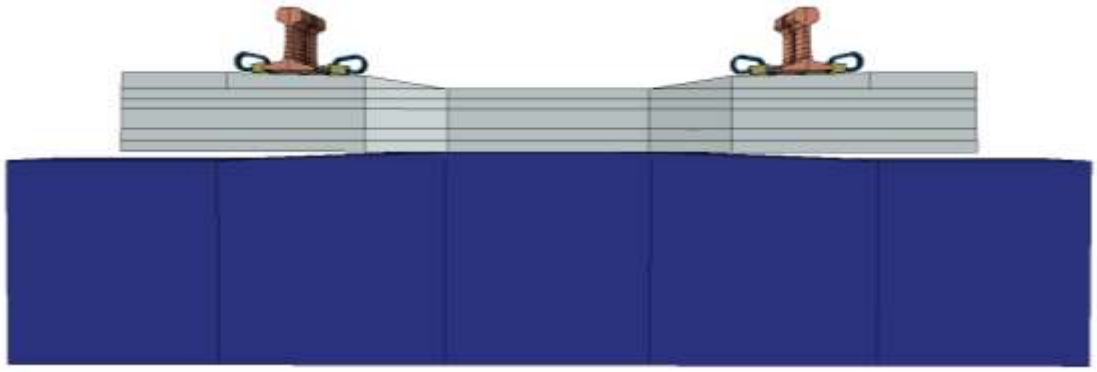

Figure 3.3 Layout of the FE model with exaggerated gap under rail-seat regions

To evaluate the effect of support conditions on the behavior of crosstie, the relationship between the vertical load and midspan concrete flexural stress was generated and shown in Figure 3.4. Due to prestress release, a compressive stress of 16.7 MPa (2421 psi) was applied at the top surface of crosstie midspan. When there was no gap between the crosstie and the ballast, the crosstie performed as a beam on elastic foundation. The top-surface concrete flexural stress at midspan gradually decreased and remained compressive under the full vertical load. However, when there was initial gap before loading, the crosstie performed as a beam that was firmly supported at the midspan and cantilevered over the two ends. The midspan concrete flexural stress on the top surface rapidly increased until the bottom of concrete was in contact with the ballast. With a gap of 3.81 mm (0.15 in), the identical load resulted in tensile cracking at the midspan of concrete crosstie. At the same time, the maximum compressive stress of concrete took place at the shoulder insert, as shown in Figure 3.5.

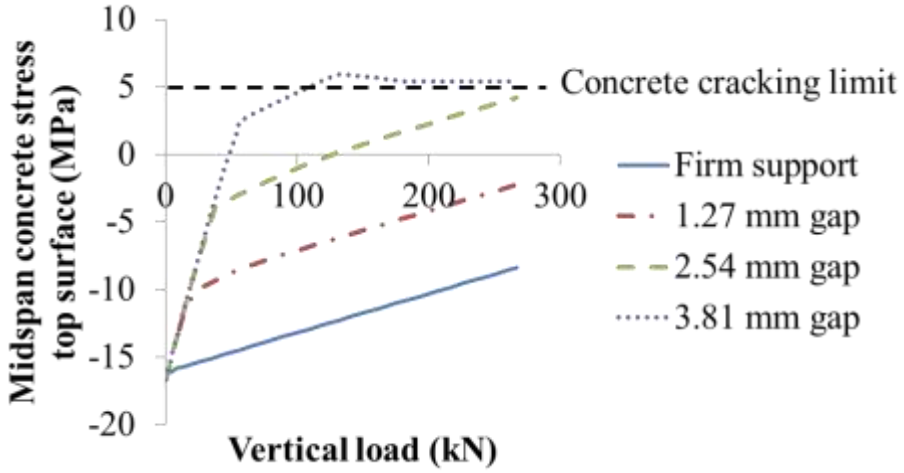

Figure 3.4 Relationship between vertical loading and concrete crosstie midspan tensile stress

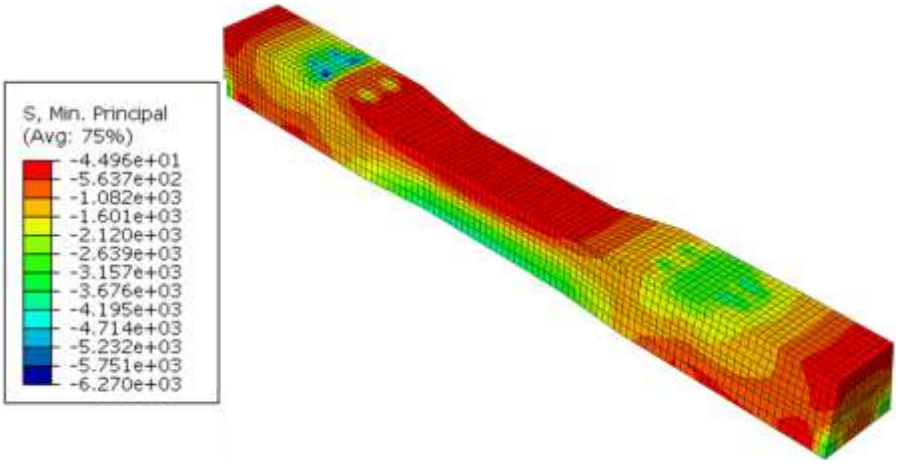

Figure 3.5 Compressive stress contour of loaded concrete crosstie with 3.81 mm (0.15 in) gap between concrete crosstie and ballast (unit: psi, 1 psi = 0.007 MPa)

In this parametric study, it can be observed that gaps between concrete crossties and ballast at the rail-seat region considerably increased the flexural demand at crosstie center. For the type of prestressed concrete crosstie in this study, a gap of 2.54 mm (0.1 in) is the threshold for allowable gap size, and any larger gap between the crosstie and ballast at the rail-seat region will result in tensile cracking at crosstie midspan. Although center binding rises as a structural problem in concrete crosstie, a possible solution to the problem is more related to the ballast surface profile than to the design of the concrete crosstie. Regular track surfacing work including tamping, stoneblowing, or undercutting eliminates gaps between concrete crosstie and ballast, and provide desirable uniform support condition for the crosstie (Lutch et al. 2009).

3.2 Parametric Studies of Critical Design Parameters

To develop a mechanistic design approach, it is critical to quantify the wheel load path under different loading scenarios and different design of track structures. However, based on the literature review there is a lack of knowledge for the effect of track design parameters on the distribution of wheel loads. To investigate the effect of and interaction between some critical design parameters on the performance of the concrete crosstie and fastening system, the FE model was used to execute a series of parametric studies. The design of parametric study is summarized in Table 3.1.

Table 3.1 Design of the parametric study of critical design parameters

		Range	Base value
Input	Crosstie spacing (m)	0.51~0.76	0.61
	Rail-pad and plate-concrete COF	0.12~1.0	0.3
	Pad elastic modulus (MPa)	27.58~2758	52
	Insulator elastic modulus (MPa)	2758~13790	3034
Output	Rail head lateral displacement		
	Shoulder bearing force at the loaded rail seat		
	Pad friction force at the loaded rail seat		
	Vertical rail seat load		
Loading scenarios	Loading scenario 1: V=178 kN, L=45 kN		
	Loading scenario 2: V=178 kN, L=89 kN		
	Loading scenario 3: V=178 kN, L=134 kN		
	Loading scenario 4: V=45 kN, L=22 kN		
	Loading scenario 5: V=89 kN, L=45 kN		
	Loading scenario 6: V=133 kN, L=66 kN		

Six loading scenarios were considered to simulate the loading conditions on curved track with varying degrees of curvature and loading magnitudes. Considering a 1401 kN (315 kip) GRP rail car with a vertical wheel load of 178 kN (40 kips), loading scenarios 1-3 were designed to look into the effect of different L/V ratios. In addition, loading scenarios 4-6 were designed to investigate the effect of different loading magnitude, and these three loading scenarios maintained an L/V ratio of 0.5. The coefficient of friction (COF) at the rail-pad interface and plate-concrete interface were combined and is discussed in detail in the following section. The ranges of input parameters were determined based on reference about tribology and polymer material property (Yamaguchi 1990, Hepburn 1982, Harper 1996) and conversations with experts in track component engineering. The same input and output parameters were studied under different loading scenarios, and the parameters that were not included were held constant

as in the field experimentation. Examples of constant parameters were track substructure stiffness and crosstie prestressing strand distribution. The definitions of output are shown in Figure 4.6. To evaluate the interactions of the design parameters (i.e. input) that were potentially significant, the parametric study was divided into two phases for each loading scenario. In the first phase, a full factorial design of cases was generated at the maximum and minimum values of the design space. Based on the FE model output, an analysis of variance (ANOVA) was used to determine the interaction of design parameters that are statistically significant (Scheffe 1999). In the second phase of this work, more cases were generated to further investigate significant input interactions.

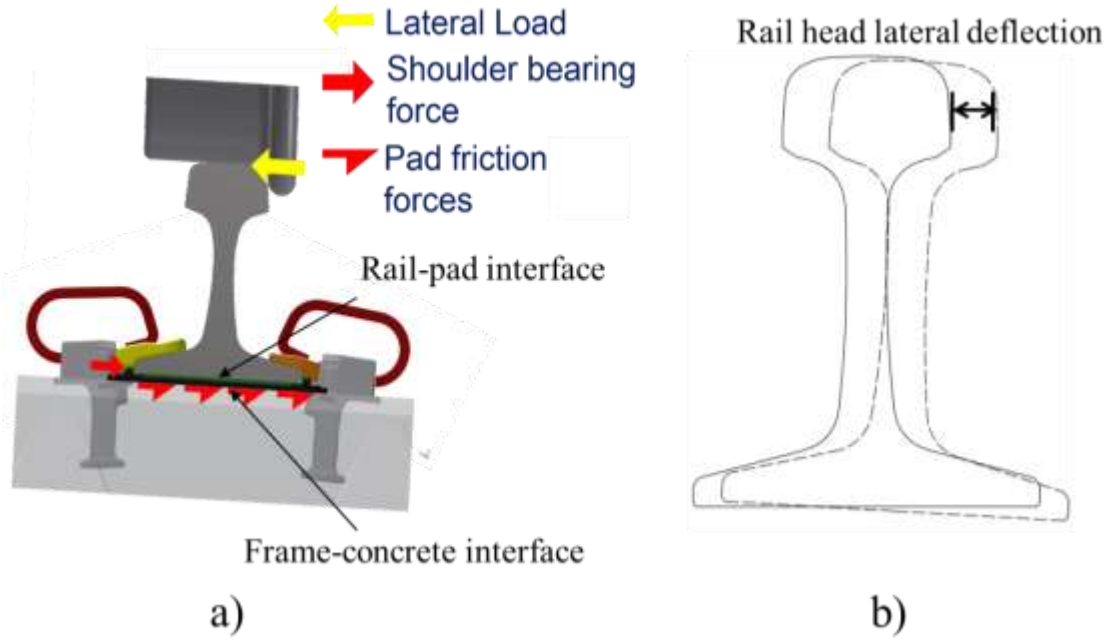

Figure 3.6 Illustration of FE model output in the parametric study: a) shoulder bearing force and pad friction force at the loaded rail seat and b) rail head lateral deflection

3.2.1 Preliminary parametric study of the rail base frictional interaction in the fastening system

Before the comprehensive parametric study was performed, the FE model was used in a preliminary parametric study on the effect of frictional interactions in the fastening system. The COF at the rail-pad interface and the plate-concrete interface were used as input variables, and select outputs related to the fastening system performance under lateral wheel loads were extracted, as shown in Table 3.2. A vertical wheel load of 178 kN (40 kips) and a lateral wheel load of 89 kN (20 kips) was used for all cases.

Table 3.2 Design of preliminary parametric study on frictional interaction

		Range
Input	Pad-rail COF	0.12～1.00
	Frame-concrete COF	0.15～1.00
Output	Rail head lateral displacement Shoulder bearing force at the loaded rail seat Pad friction force at the loaded rail seat	
Loading scenario	V=178 kN, L=89 kN	

In the parametric study, both COF at the two interfaces were varied to evaluate their interaction. The two lines in each part of Figure 3.7 indicate the cases with different frame-concrete COF. In Figure 3.7, it can be observed that within a range, the rail pad frictional force increased with higher COF, and both the shoulder bearing force and rail-head lateral deflection decreased with higher COF. At higher COF the model output was not as sensitive to the change in COF.

Under lateral wheel loads, the relative sliding between rail base and concrete could be divided into three parts: 1) the relative sliding between rail and the rail pad, 2) between the abrasion plate and concrete, and 3) the shear deformation of the entire rail pad assembly. As the rail pad was embedded into the abrasion plate, the relative sliding between the rail pad and abrasion plate was assumed to be insignificant. The COF at the two interfaces served as the threshold for the linear friction-sliding relationship. Under higher lateral load, the frictional force remained at the maximum magnitude while the relative sliding continued to increase. As a result of this behavior, it was reasonable to approximate the frictional stiffness at the bottom of rail base as springs in series, and the threshold of linear behavior was determined (i.e. governed) by the lower COF of the two interfaces.

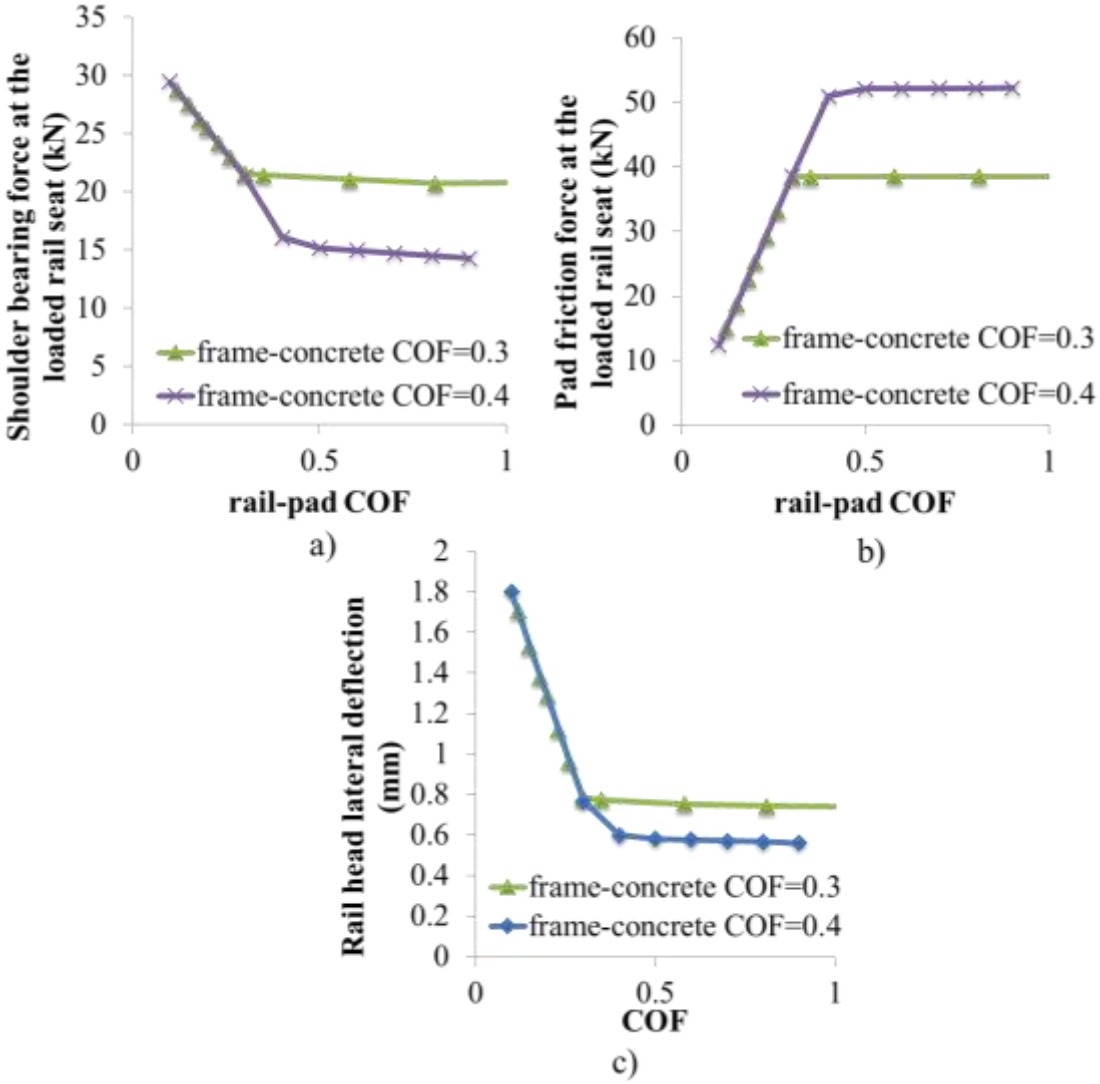

Figure 3.7 Results from two-variable parametric studies focusing on a) shoulder bearing force, b) rail pad friction force, and c) the rail head lateral deflection

In Figure 3.7, the slopes of the two lines changed at different COF magnitude, which were 0.3 and 0.4, respectively. The location of different thresholds agreed with the frame-concrete COF of the cases. When the rail-pad COF was lower than the frame-concrete COF, it governed the system response, and identical response was observed between cases of different frame-concrete COF. However, when the rail-pad COF exceeded the frame-concrete COF, the frame-concrete COF governed the system response, which was not sensitive to the change of rail-pad COF. Considering this effect, the rail-rail pad COF and frame-concrete COF were combined into one variable, and identical COF were defined at the two interfaces for further parametric study.

3.2.2 Determination of critical input interaction

To determine the input interactions that were statistically significant, the FE model was used to run model iterations that were generated using a full factorial design (Box et al. 1978). In total, four input variables were included in the parametric study under each loading scenario, and 96 cases ($2^4 * 6 = 96$) were generated. Two levels were considered for each input variable, representing its minimum and maximum value.

After the cases were generated, the statistical software R (Venables et al. 2002) was used for ANOVA. A statistical model was built for each output, and through an ANOVA, p-values (Walpole et al. 1993) were calculated for each input variable and its interactions. Lower p-values indicate that the corresponding input or input interaction is more statistically significant for a certain output, and the threshold p-value to study the input interaction was determined as 0.05 (Walpole et al. 1993). In addition, the statistical models were built considering the hierarchy of variables (Faraway 2002). The input variables were defined as factorial, and they were first introduced in the statistical model without their interaction terms. Based on the result of ANOVA, input variables with a p-value larger than 0.05 were deemed insignificant and were removed from the model. After this step, only the second-order interactions of remaining input variables were added to the model and tested for significance. After the insignificant terms were removed from the statistical model, higher-order interaction terms were added until all of the combinations were exhausted.

The results of ANOVA for the six loading scenarios are summarized in Table 3.3 and Table 3.4. The p-values of significant interactions are marked in bold. Some p-values were left blank as the corresponding input or lower-order input interaction was not significant for the given output. It can be observed that all of the second-order interactions of input variables were significant for at least one of the outputs, and none of the third-order interactions were significant to any of the output. The elastic modulus of the insulator and its interaction with other input were not included as they were not statistically significant for any of the four outputs. Comparing the result of ANOVA under different loading scenarios, it can be observed that the sensitivity of the track structure performance to the same design parameters changes under different loading scenarios. Considering this result, more cases were generated to investigate all of the second-order interactions of the three input variables. The result of phase 2 parametric study is discussed based on different loading scenarios in the following section. As similar result is observed in loading scenario 2, 3, 5 and 6, the parametric study result under loading scenario 2 is shown as an example.

Table 3.3 ANOVA results for loading scenarios 1-2

Loading Scenario 1

Vertical load = 178 kN, Lateral load = 44 kN

Interaction	P-value			
	Rail head lateral deflection	**Shoulder bearing force**	**Rail pad frictional force**	**Vertical rail seat load**
Spacing: COF	N/A	N/A	**3.7E-02**	**4.0E-03**
Spacing: Pad modulus	**4.9E-04**	**4.6E-03**	**7.1E-04**	N/A
COF: Pad modulus	**4.8E-06**	**6.7E-07**	**3.7E-10**	**2.0E-03**
Spacing: COF: Pad modulus	N/A	N/A	N/A	N/A

Loading Scenario 2

Vertical load = 178 kN, Lateral load = 89 kN

Interaction	P-value			
	Rail head lateral deflection	**Shoulder bearing force**	**Rail pad frictional force**	**Vertical rail seat load**
Spacing: COF	**1.3E-04**	N/A	N/A	**7.0E-05**
Spacing: Pad modulus	**1.6E-03**	N/A	N/A	N/A
COF: Pad modulus	**5.1E-06**	**4.2E-06**	**6.7E-06**	**3.5E-09**
Spacing: COF: Pad modulus	N/A	N/A	N/A	N/A

Table 3.4 ANOVA results for loading scenarios 3-4

Loading scenario 3

Vertical load = 178 kN, Lateral load = 133 kN

Interaction	P-value			
	Rail head lateral deflection	**Shoulder bearing force**	**Rail pad frictional force**	**Vertical rail seat load**
Spacing: COF	**4.4E-08**	N/A	N/A	**3.6E-07**
Spacing: Pad modulus	**1.7E-04**	N/A	N/A	7.9E-01
COF: Pad modulus	**4.2E-06**	**2.2E-10**	**4.1E-06**	**1.2E-12**
Spacing: COF: Pad modulus	N/A	N/A	N/A	N/A

Spacing: Concrete crosstie spacing
COF: The coefficient of friction at the rail-pad interface and the frame-concrete interface
Pad modulus: The elastic modulus of rail pad

Loading scenario 4

Vertical load = 44 kN, Lateral load = 22 kN

Interaction	P-value			
	Rail head lateral deflection	**Shoulder bearing force**	**Rail pad frictional force**	**Vertical rail seat load**
Spacing: COF	N/A	**9.2E-03**	N/A	**1.2E-02**
Spacing: Pad modulus	**9.9E-03**	**2.8E-02**	N/A	N/A
COF: Pad modulus	**4.9E-07**	**2.1E-06**	**5.8E-04**	**4.0E-03**
Spacing: COF: Pad modulus	N/A	N/A	N/A	N/A

Table 3.5 ANOVA results for loading scenarios 5-6

Loading scenario 5

Vertical load = 89 kN, Lateral load = 44 kN

Interaction	P-value			
	Rail head lateral deflection	**Shoulder bearing force**	**Rail pad frictional force**	**Vertical rail seat load**
Spacing: COF	**1.4E-02**	N/A	N/A	**4.6E-03**
Spacing: Pad modulus	**5.0E-03**	N/A	N/A	N/A
COF: Pad modulus	**6.6E-06**	**2.4E-04**	**3.0E-05**	**1.0E-06**
Spacing: COF: Pad modulus	N/A	N/A	N/A	N/A

Loading scenario 6

Vertical load = 133 kN, Lateral load = 67 kN

Interaction	P-value			
	Rail head lateral deflection	**Shoulder bearing force**	**Rail pad frictional force**	**Vertical rail seat load**
Spacing: COF	**1.1E-03**	N/A	N/A	**2.0E-04**
Spacing: Pad modulus	**2.3E-03**	N/A	N/A	N/A
COF: Pad modulus	**8.7E-06**	**2.0E-05**	**7.3E-06**	**2.1E-09**
Spacing: COF: Pad modulus	N/A	N/A	N/A	N/A

Spacing: Concrete crosstie spacing
COF: The coefficient of friction at the rail-pad interface and the frame-concrete interface Pad modulus: The elastic modulus of rail pad

3.2.3 Results from loading scenario 1: V = 178 kN, L= 44 kN, L/V = 0.25

Under loading scenario 1, nine input interactions were determined as significant, and 64 cases (i.e. FE model runs) were generated to investigate the interaction of input variables. The results are summarized by relevant output variables in the following sections.

3.2.3.1 Output: rail head lateral deflection

The rail head lateral deflection varied with respect to the interactions of rail pad elastic modulus and COF, and rail pad elastic modulus and crosstie spacing (Figure 3.8). Rail head lateral deflection generally decreased with higher rail pad elastic modulus, higher COF, and closer crosstie spacing. Compared to COF and rail pad elastic modulus, crosstie spacing had relatively little effect on the variation of rail head lateral deflection. The COF defined in the FE model affected the threshold of the linear friction-sliding relationship at the rail base, and minor differences in rail head deflection were observed between cases of high COF as the ratio between the rail pad friction force and the normal force at the loaded rail seat was smaller than the defined COF. In addition, the rail head lateral deflection gradually converged to a set number at high values of rail pad elastic modulus. More significant interaction (lines of different slopes) was observed between rail pad elastic modulus and COF than between rail pad elastic modulus and crosstie spacing. This agreed with the fact that the COF-pad modulus interaction had a smaller p-value than the pad modulus-spacing interaction.

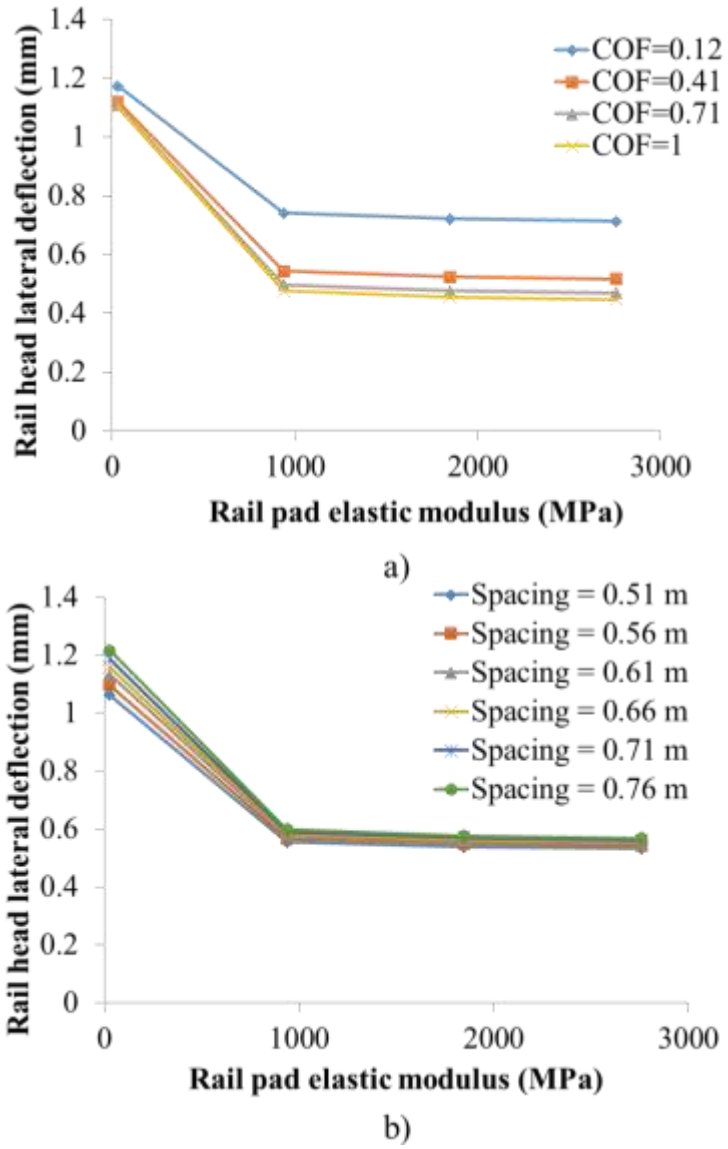

Figure 3.8 Variation of rail head lateral deflection with respect to the interaction of a) rail pad elastic modulus and COF, and b) rail pad elastic modulus and crosstie spacing (loading scenario 1: V=178 kN, L=44 kN)

3.2.3.2 Output: shoulder bearing force at the loaded rail seat

The variation of shoulder bearing force at the rail seat under the point of load application with respect to the interaction of rail pad elastic modulus and COF, and rail pad elastic modulus and crosstie spacing is shown in Figure 3.9. The shoulder bearing force at the loaded rail seat gradually decreased with higher rail pad elastic moduli, higher COF, and closer crosstie spacing. The crosstie spacing had relatively small impact on the variation of the shoulder bearing force, when compared to the other two input variables (rail pad elastic modulus and COF). In other words, the shoulder bearing force at the loaded rail seat is affected by the design of the fastening system (COF and rail pad elastic modulus)

more than the global system configuration (crosstie spacing). In addition, the shoulder bearing force gradually converged to a set value at high rail pad elastic moduli and high COF. At the same time, more significant interaction was observed between the rail pad elastic modulus and the COF than between the rail pad elastic modulus and crosstie spacing. Both the rail pad elastic modulus and the COF determined the lateral frictional stiffness at the bottom of rail base, and crosstie spacing had minimal impact on the lateral load path through the fastening system.

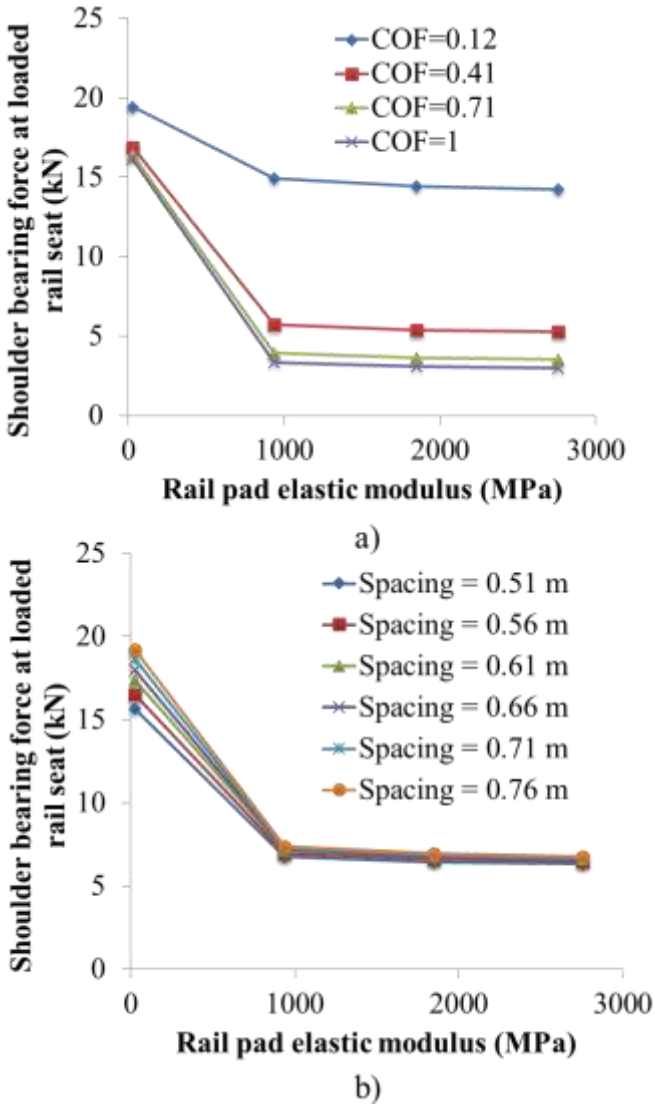

Figure 3.9 Variation of shoulder bearing force at the loaded rail seat with respect to the interaction of a) rail pad elastic modulus and COF, and b) rail pad elastic modulus and crosstie spacing (loading scenario 1: V=178 kN, L=44 kN)

3.2.3.3 Output: rail pad friction force at the loaded rail seat

The variation of rail pad friction force at the rail seat under the point of load application with respect to the interaction of rail pad elastic modulus and COF, rail pad elastic modulus and crosstie spacing, and COF and crosstie spacing is shown in Figure 3.10. The rail pad friction force gradually decreased with lower rail pad elastic modulus, lower COF, and closer crosstie spacing. ANOVA indicated that the rail pad friction force at the loaded rail seat was significantly affected by all three second-order input interactions. However, it was also observed that the relationship between crosstie spacing and rail pad friction force was linear, and crosstie spacing had minor interaction with the other two input variables (rail pad elastic modulus and COF). The rail pad elastic modulus and COF had larger impact on the rail pad friction force at low load magnitudes, and the impact gradually reduced at higher load magnitudes.

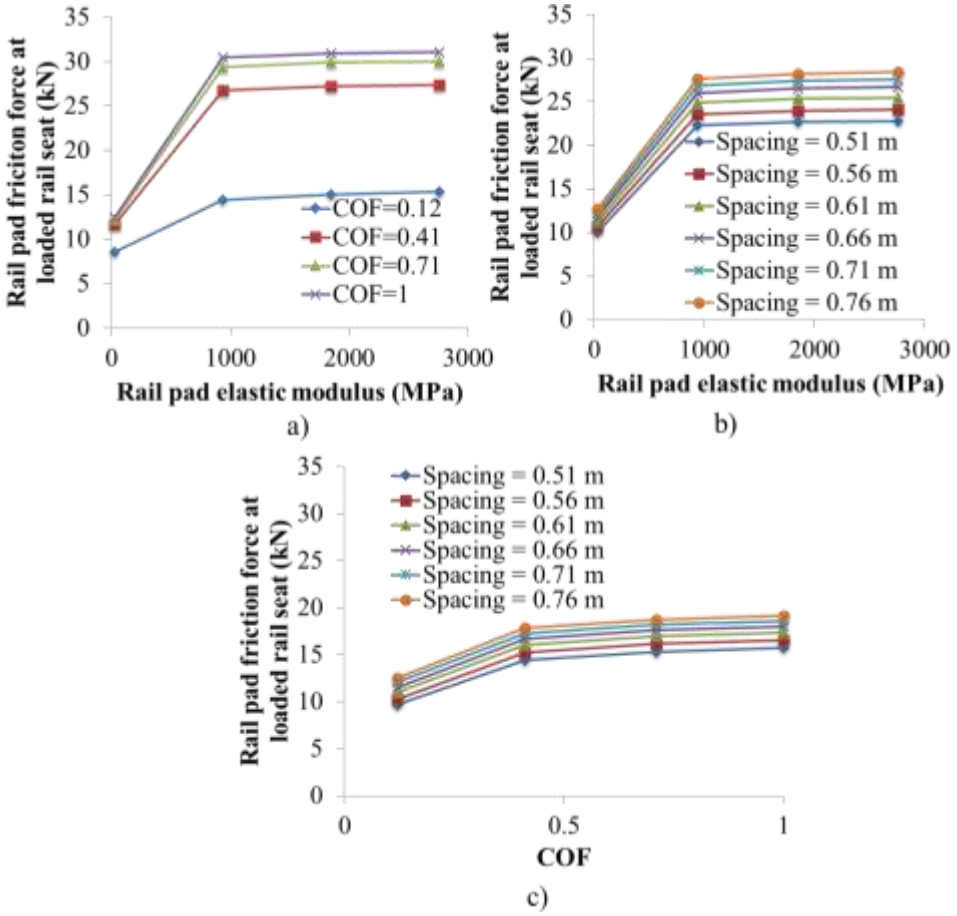

Figure 3.10 Variation of rail pad friction force at the loaded rail seat with respect to the interaction of a) rail pad elastic modulus and COF, b) rail pad elastic modulus and crosstie spacing, and c) COF and crosstie spacing (loading scenario 1: V=178 kN, L=44 kN)

3.2.3.4 Output: vertical rail seat load

The variation of vertical rail seat load at the rail seat under the point of load application with respect to the interaction of rail pad elastic modulus and COF, and COF and crosstie spacing, is shown in Figure 3.11. The vertical rail seat load gradually decreased with smaller rail pad elastic modulus, lower COF, and closer crosstie spacing. It was observed that the relationship between crosstie spacing and vertical rail seat load was linear, and the crosstie spacing had a greater impact on the vertical rail seat load than the other two input variables. The rail pad elastic modulus affected the vertical rail seat load as it determined the vertical compression of the rail pad. The COF also affected the vertical rail seat load as the friction forces at the rail-pad interface and plate-concrete interface restrained the lateral expansion of the pad assembly and altered the effective compressive stiffness of the rail pad assembly.

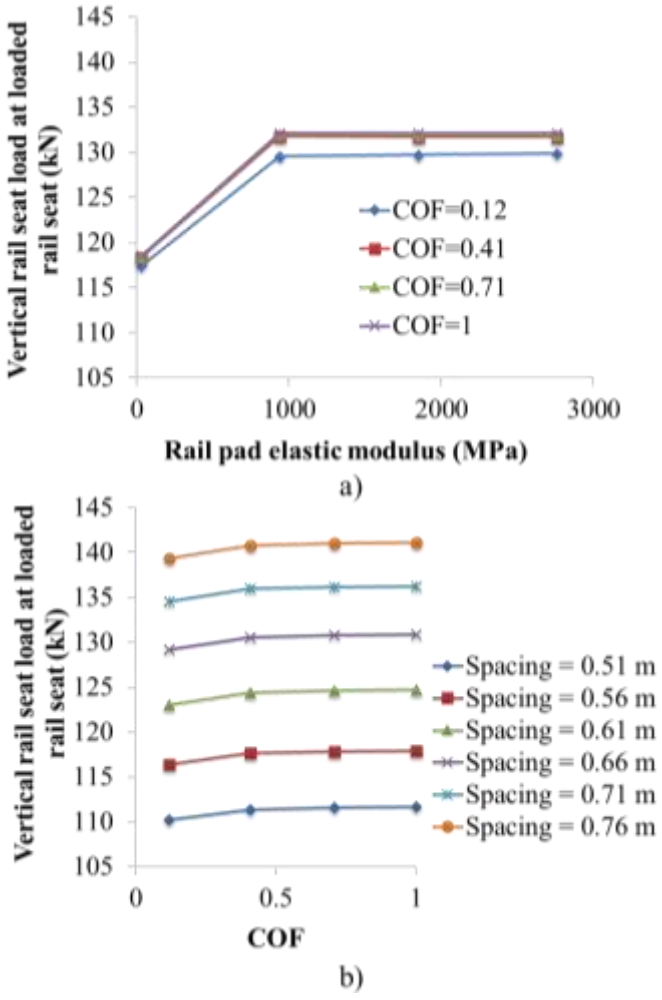

Figure 3.11 Variation of vertical rail seat load at the loaded rail seat with respect to the interaction of a) rail pad elastic modulus and COF, and b) COF and crosstie spacing (loading scenario 1: V=178 kN, L=44 kN)

3.2.4 Results from loading scenario 2: V = 178 kN, L= 89 kN, L/V=0.5

As similar parametric study results are observed in loading scenario 2, 3, 5 and 6, the analysis for loading scenario 2 is presented in this section. Under loading scenario 2, seven interactions were determined as significant, and 64 cases were generated investigate the interactions using the FE model. The results are summarized by relevant outputs in the following sections.

4.2.4.1 Output: rail head lateral deflection

The variation of rail head lateral deflection with respect the interaction of rail pad elastic modulus and COF, rail pad elastic modulus and crosstie spacing, and COF and crosstie spacing, is shown in Figure 3.12. For loading scenario 2, the interaction of various input on rail head lateral deflection was similar to what was noted in loading scenario 1. The rail head lateral deflection decreased with higher rail pad elastic modulus, higher COF, and closer crosstie spacing. The rail head lateral deflection gradually converged to a set value at high rail pad elastic moduli and high COF. The major interaction of input variables was observed between the rail pad elastic modulus and COF, and minor interaction was observed between the crosstie spacing and the other two input variables.

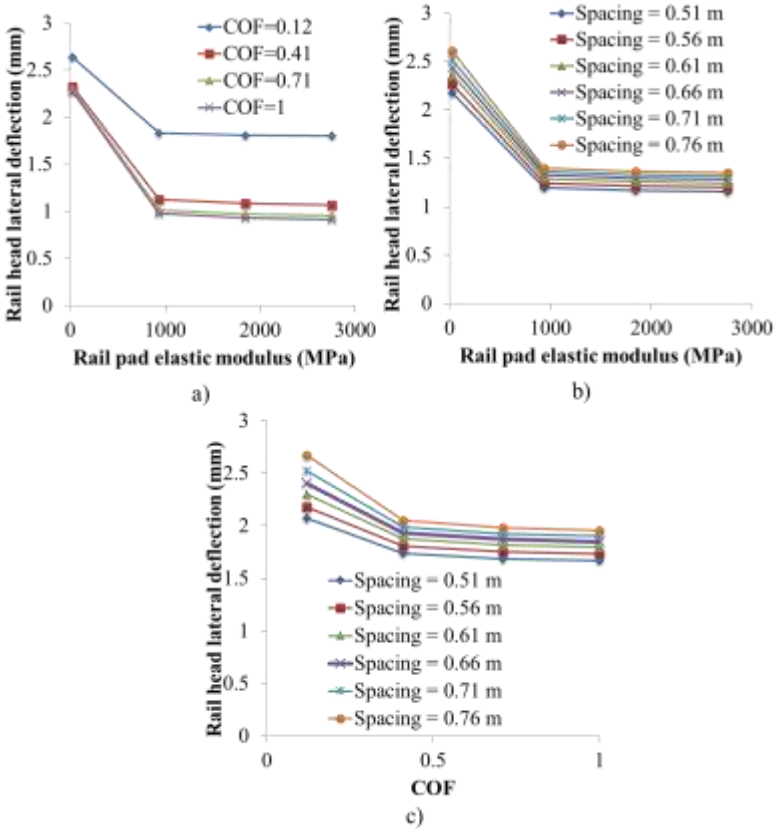

Figure 3.12 Variation of rail head lateral deflection with respect to the interaction of a) rail pad elastic modulus and COF, b) rail pad elastic modulus and crosstie spacing, and c) COF and crosstie spacing (loading scenario 2, V=178 kN, L=89 kN)

3.2.4.2 Output: shoulder bearing force at the loaded rail seat

Unlike loading scenario 1, the only significant interaction of input related to shoulder bearing force at the loaded rail seat in loading scenario 2 was between the rail pad elastic modulus and COF (Figure 4.13). The shoulder bearing force at the loaded rail seat decreased with higher rail pad elastic moduli and higher COF. In addition, the rail pad elastic modulus had larger impact on the shoulder bearing force at higher COF values. At a lower COF, limited friction force developed at the rail-pad interface and the plate-concrete interface, and as a result little difference in rail pad shearing existed between cases of different rail pad elastic moduli. Therefore the shoulder bearing force was not significantly affected. At a higher COF, linear friction-sliding relationship existed at the surfaces of the rail pad assembly, and the shearing of rail pad varied within a larger range of values, which affected the shoulder bearing force.

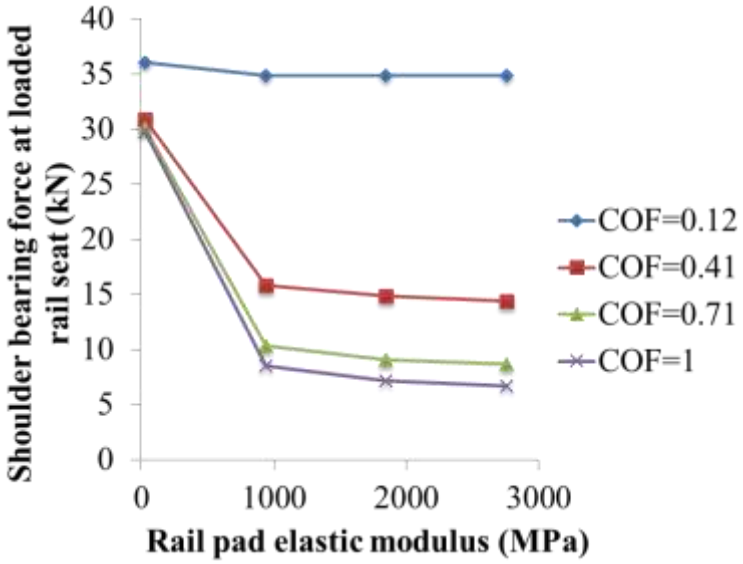

Figure 3.13 Variation of shoulder bearing force at the loaded rail seat with respect to the interaction of rail pad elastic modulus and COF (loading scenario 2, V=178 kN, L=89 kN)

3.2.4.3 Output: rail pad friction force at the loaded rail seat

The variation of rail pad friction force with respect to the interaction of rail pad elastic modulus and COF is shown in Figure 3.14. The result of ANOVA indicated that in loading scenario 2 the only significant input interaction about rail pad friction force was between the rail pad elastic modulus and COF. The result of input interaction about rail pad friction force was closely aligned with those relating to shoulder bearing force. The rail pad friction force at the loaded rail seat decreased with lower rail pad elastic modulus and lower COF. In addition, the rail pad elastic modulus had larger impact on the rail pad friction force at high COF, and the impact decreased at lower COF.

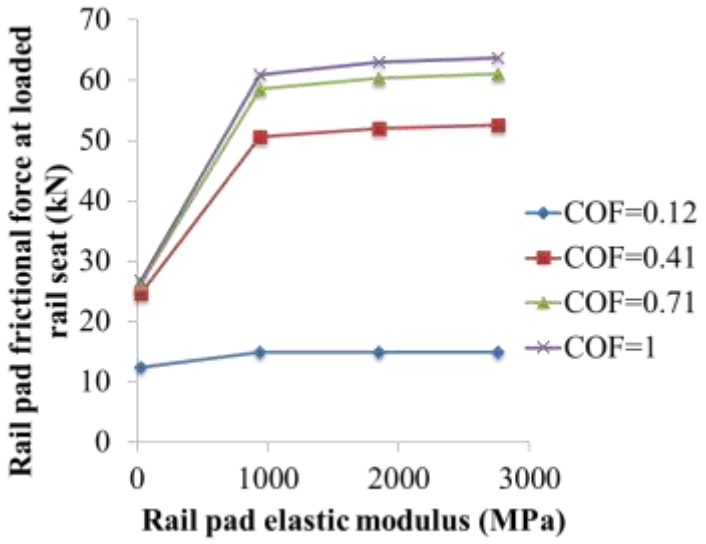

Figure 3.14 Variation of rail pad friction force at the loaded rail seat with respect to the interaction of rail pad elastic modulus and COF (loading scenario 2, V=178 kN, L=89 kN)

3.2.4.4 Output: vertical rail seat load

The variation of vertical rail seat load with respect to the interaction of rail pad elastic modulus and COF, and COF and crosstie spacing is shown in Figure 3.15. The vertical rail seat load decreased with lower rail pad elastic modulus, lower COF, and closer crosstie spacing. In addition, the crosstie spacing had a larger impact on the vertical rail seat load than the other two input variables. Although the two interactions in Figure 3.15 were determined as statistically significant, they were not as significant as other interactions that were studied. The vertical rail seat load converged to a set value at high rail pad elastic modulus and high COF. In addition, it was observed that the relationship between crosstie spacing and the vertical rail seat load was approximately linear, and minor interaction was noted between it and other input variables.

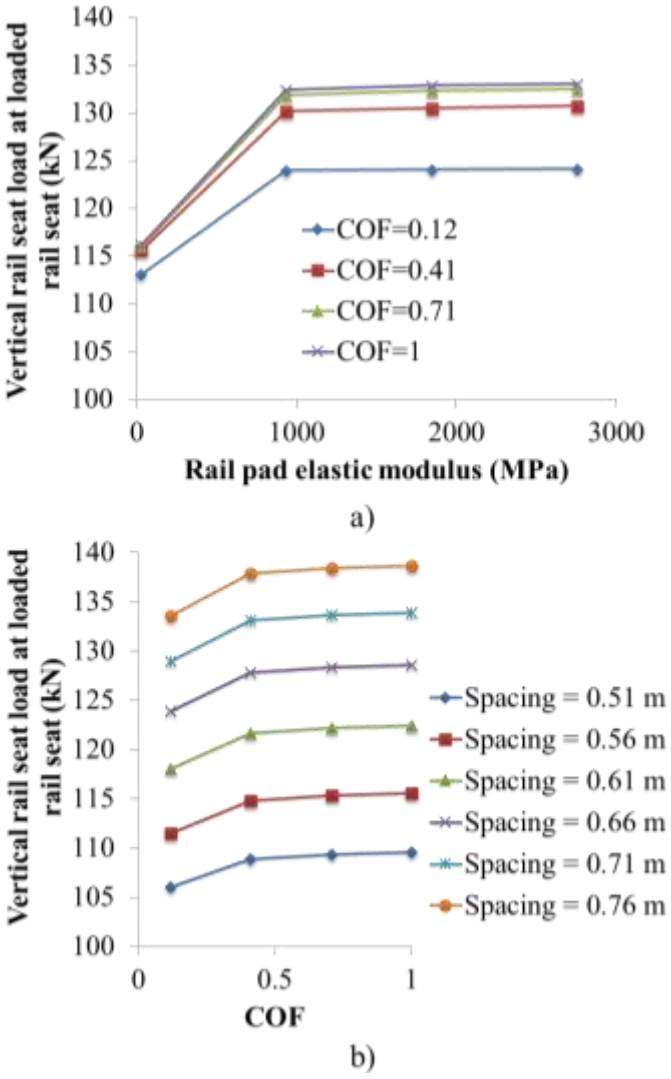

Figure 3.15 Variation of vertical rail seat load at the loaded rail seat with respect to the interaction of a) rail pad elastic modulus and COF, and b) COF and crosstie spacing (loading scenario 2, V=178 kN, L=89 kN)

3.2.5 Results from loading scenario 4: V = 44 kN, L= 22 kN, L/V=0.5

Under loading scenario 4, eight interactions were determined to be statistically significant. While the ratio between the vertical and lateral wheel load is the same in loading scenario 4 as in loading scenario 2, as the magnitude of vertical wheel load is much smaller, the distribution of the vertical wheel load is more affected by the clamping force at each rail seats. As a result, the sensitivity of the track structure performance to the critical design parameters are different from what is observed under loading scenario 2. 64 cases were generated based on the FE model to investigate the interaction of the inputs, and the results were summarized based on the relevant output variables in the following sections.

3.2.5.1 Output: rail head lateral deflection

The variation of rail head lateral deflection with respect to the interaction of rail pad elastic modulus and COF, and COF and crosstie spacing, is shown in Figure 3.16. The rail head lateral deflection decreased with higher rail pad elastic modulus, higher COF, and closer crosstie spacing. The result of rail head lateral deflection in loading scenario 3 was quite similar to loading scenario 1 except for a difference in magnitude. The rail head lateral deflection converged to a set value at high rail pad elastic moduli and high COF values. In addition, the crosstie spacing had minor interaction with rail pad elastic modulus and the COF, and the relationship between crosstie spacing and the rail head lateral deflection was approximately linear.

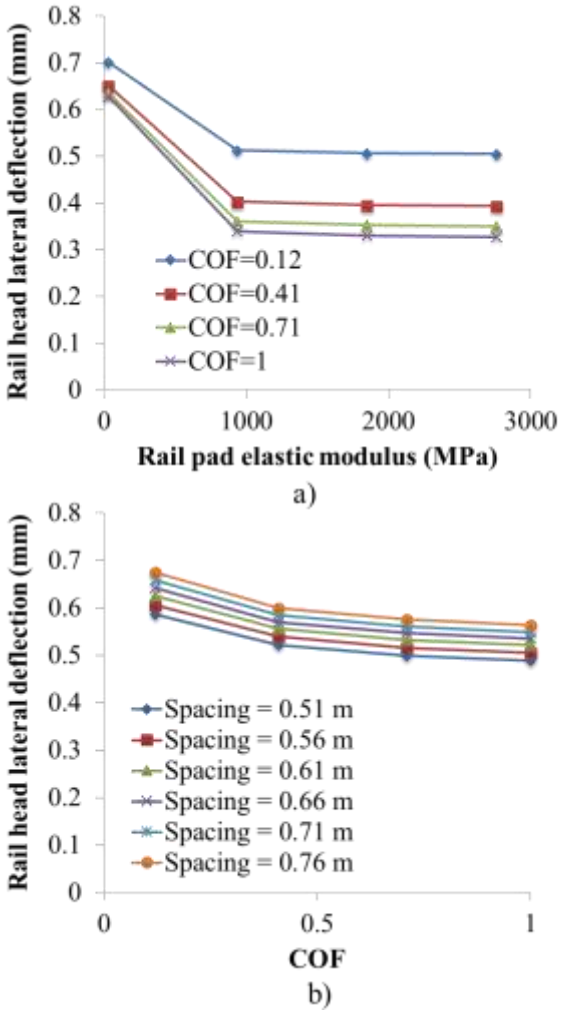

Figure 3.16 Variation of rail head lateral deflection with respect to the interaction of a) rail pad elastic modulus and COF, b) COF and crosstie spacing (loading scenario 4, V=44 kN, L=22 kN)

3.2.5.2 Output: shoulder bearing force at the loaded rail seat

The variation of shoulder bearing force with respect to the interaction of rail pad elastic modulus and COF, COF and crosstie spacing, and crosstie spacing and rail pad elastic modulus is shown in Figure 3.17. The shoulder bearing force at the loaded rail seat decreased with higher rail pad elastic moduli, higher COF values and closer crosstie spacing. In addition, the shoulder bearing force gradually converged to a set value at high rail pad elastic moduli and high COF values. It can be observed that the rail pad elastic modulus had a larger impact on the shoulder bearing force at higher COF values. Parallel lines in Figure 3.17b) and 3.17c) indicate that the interaction is minor between crosstie spacing and the other two design parameters. In other words, while the concrete crossties are installed at different spacing, the effect of COF and rail pad elastic modulus on the change of shoulder bearing force at the loaded rail seat is similar.

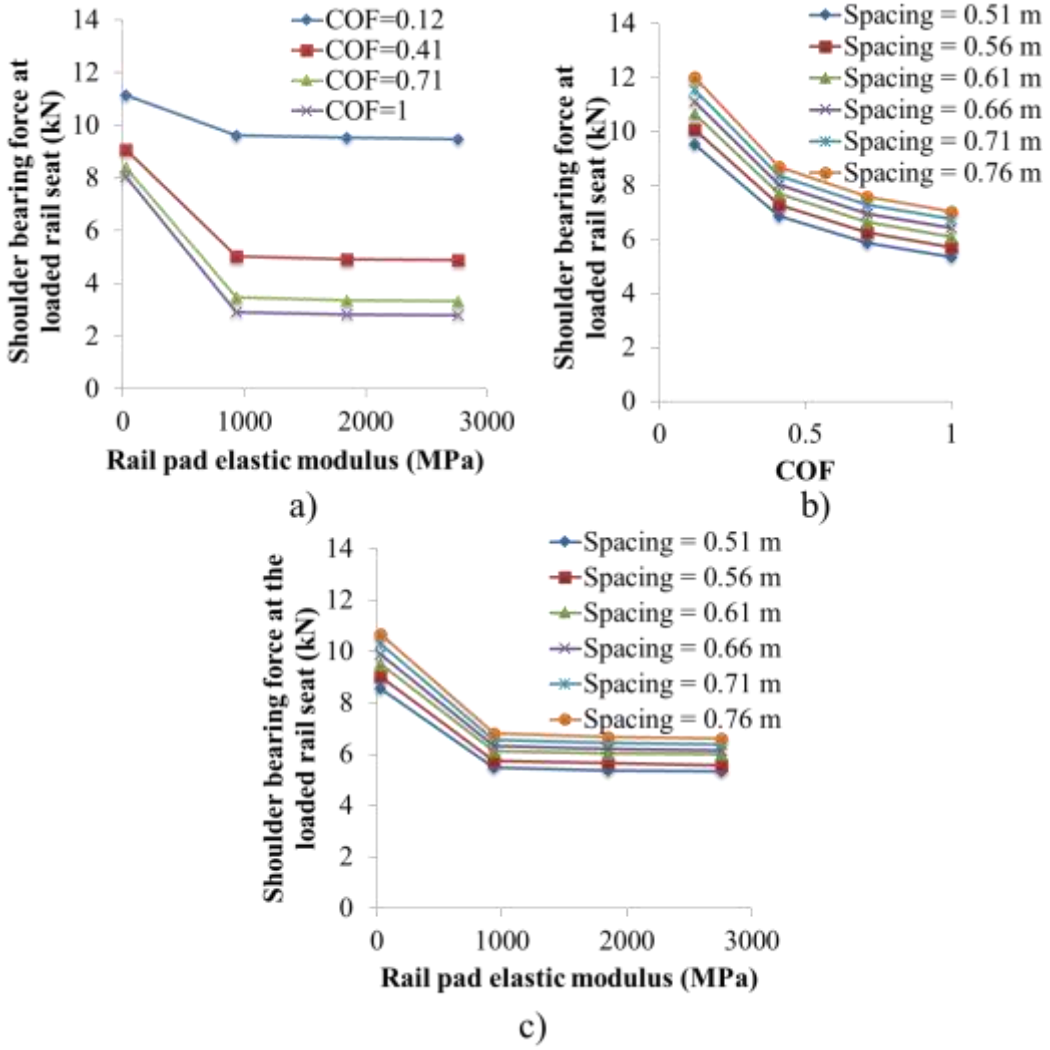

Figure 3.17 Variation of shoulder bearing force at the loaded rail seat with respect to the interaction of a) rail pad elastic modulus and COF, b) COF and crosstie spacing, and c) rail pad elastic modulus and crosstie spacing (loading scenario 4, V=44 kN, L=22 kN)

3.2.5.3 Output: rail pad friction force at the loaded rail seat

The variation of rail pad friction force with respect to the interaction of rail pad elastic modulus and COF is shown in Figure 3.18. The rail pad friction force decreased with lower rail pad elastic moduli and lower COF values. In addition, the rail pad friction force converged to a set value at high rail pad elastic moduli and high COF values. Similar to the result regarding shoulder bearing force in loading scenario 4, the rail pad elastic modulus had larger impact on the rail pad friction force at higher COF.

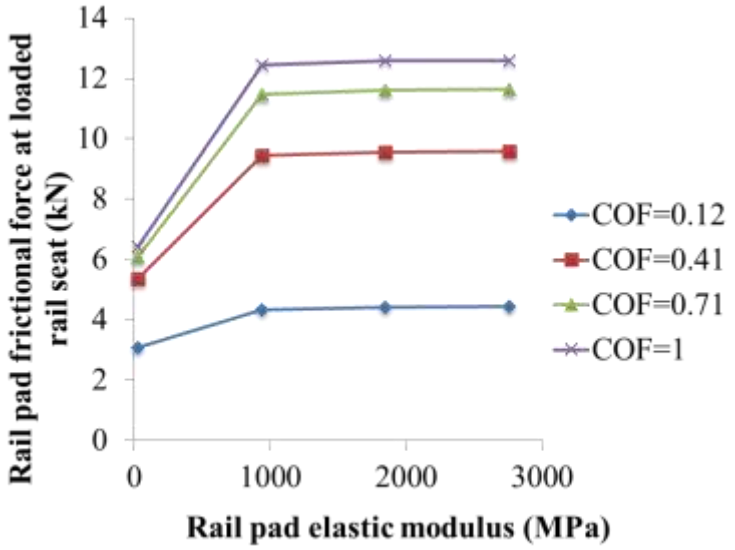

Figure 3.18 Variation of rail pad friction force at the loaded rail seat with respect to the interaction of rail pad elastic modulus and COF (loading scenario 4, V=44 kN, L=22 kN)

3.2.5.4 Output: vertical rail seat load

The variation of vertical rail seat load with respect to the interaction of rail pad elastic modulus and COF, and COF and crosstie spacing, is shown in Figure 3.19. The vertical rail seat load decreased with lower rail pad elastic modulus, lower COF, and closer crosstie spacing. In addition, the vertical rail seat load converged to a set value at high rail pad elastic moduli and high COF values. Similar to other loading scenarios, the crosstie spacing had a larger impact on the vertical rail seat load than the rail pad elastic moduli and COF values, but it had limited interaction with the other two input variables.

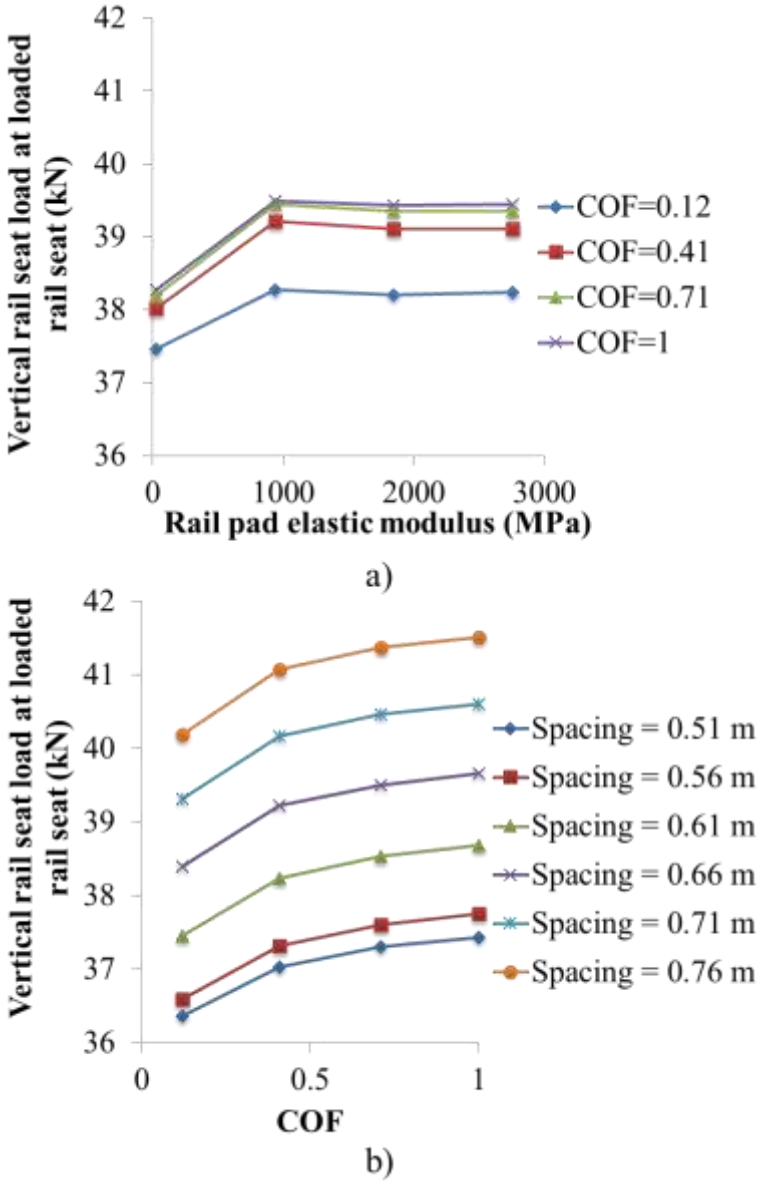

Figure 3.19 Variation of vertical rail seat load at the loaded rail seat with respect to the interaction of a) rail pad elastic modulus and COF, and b) COF and crosstie spacing (loading scenario 4, V=44 kN, L=22 kN)

SECTION 4: CONCLUSIONS AND RECOMMENDATIONS

4.1 Conclusions of the Study

The objective of this study was to further investigate the performance and design of concrete crosstie and fastening system using finite element analysis, and explore possible improvement to the current AREMA design standard. The crosstie and the fastening system are critical components of the railroad track structure, and the wheel load path from the rail head to the ballast should be clearly defined to ensure the track safety. The research necessity has been proven by the international survey that was conducted by the RailTEC at UIUC (FRA 2013) and the increasing axle load due to heavier freight traffic and higher-speed passenger rail.

Based on the parametric studies using the FE model, some conclusions can be summarized from this study:

- Under field conditions, the vertical support stiffness underneath the crossties varied considerably from one rail seat to the other. The vertical rail seat load of the loaded rail seat varied between 25% and 62.5% of the vertical wheel load. In addition, the vertical support stiffness underneath the crosstie increased considerably under higher vertical wheel load.
- The transfer length of prestressed concrete crossties gradually reduced with higher bond-slip stiffness between concrete and prestressing strands. For prestressed concrete crossties of similar dimensions, the threshold of reinforcement bond-slip stiffness to develop sufficient effective prestress at the rail-seat region is 16502 MPa/m, which is the equivalent pull-out stress divided by the reinforcement end slip.
- Gaps between the concrete crosstie and ballast at the rail-seat region considerably increase the flexural demand at the crosstie center. For the crosstie type considered in this study a gap larger than 2.54 mm (0.1 in) resulted in tensile cracking of concrete at the top surface of crosstie midspan under a vertical loading of 267 kN (60 kips).
- The elastic modulus of the fastening system insulator has little effect on the lateral load path through the fastening system.
- Compared to the COF at the rail-pad and plate-concrete interfaces, and the elastic modulus of rail pad, crosstie spacing has a very minimal impact on the performance of the fastening system under lateral wheel load.
- The COF at the rail-pad and the plate-concrete interfaces, and the elastic modulus of the rail pad significantly affect the performance of the fastening system under lateral wheel load.

- Crosstie spacing significantly affects the distribution of vertical wheel load among multiple rail seats, and the relationship between crosstie spacing and the vertical rail seat load under the point of load application is approximately linear.

In conclusion, this study provided insights on the performance and load path of the continuous railroad track structure under a combination of vertical and lateral wheel load, and proved finite element analysis to be a valuable tool in the analysis of railroad infrastructure.

4.2 Recommendation for Future Research

In this study, finite element models of the concrete crosstie and fastening system were built to investigate the performance of continuous track structure under static wheel loads. However, as a large portion of the track component failures are due to impact loading, the impact analysis of the track structure is recommended to better understand the possible difference in wheel load path between static and impact loading scenarios. In addition, the longitudinal wheel load due to braking/accelerating and thermal effect is also critical to the deformation of the track structure. In future studies it is recommended to consider the combined effect of vertical, lateral, and longitudinal wheel load on the track structure as in this study only a combination of vertical and lateral wheel load is considered. Besides, on railroad tracks, the crossties and fastening systems are usually not in perfect condition due to abrasion and fatigue. Further researches on the gradual change of track structure damage state and performance will be beneficial to determine the serviceability limit state and maintenance frequency of the railroad infrastructure. Therefore it is recommended to experimentally and numerically look into the effect of damaged track components on the system performance of the track structure.

REFERENCES

Abrishami, H. H., and Mitchell, D. (1993). "Bond Characteristics of Pretensioned Strand." *ACI Materials Journal*, 90(3), 228-235.

AREMA (2012). "Manual for Railway Engineering." *Ties*, AREMA, Lanham, MD 20706.

Du, M. M., Su, X. Z., and Zhao, Y. (2010). "Experimental Study on Bond Behavior of Ribbed Bar and Strand." *Jianzhu Cailiao Xuebao/Journal of Building Materials*, 13(2), 175-181.

FRA (2012). "Track Safety Standards Class 6 through 9." *Track and Rail and Infrastructure Integrity Compliance Manual*, Federal Railroad Administration, Washington, DC 20590.

FRA (2013). "International Concrete Crosstie and Fastening System Survey."Washington, DC 20590.

Faraway, J.J. (2002). Practical Regression and ANOVA using R.

Harper, C. A. (1996). "Handbook of Plastics, Elastomers, and Composites,." *McGraw-Hill Inc*, 2, 2.41.

Hepburn, C. (1982). *Polyurethane Elastomers*, Applied Science Publishers London.

Holste, J. R., Haynes, M., Peterman, R. J., Beck, B. T., and Wu, C.-H. J. (2014). "Tensioned Pullout Test Used to Investigate Wire Splitting Propensity in Concrete Railroad Ties." *Proc., Joint Rail Conference*, ASME, New York, NY 10016-5990.

Huang, H., and Tutumluer, E. (2011). "Discrete Element Modeling for fouled railroad ballast." *Construction and Building Materials*, 25(8), 3306-3312.

Kernes, R. G., Edwards, J. R., Dersch, M. S., Lange, D. A., and Barkan, C. P. L. (2012). "Investigation of the Dynamic Frictional Properties of a Concrete Crosstie Rail Seat and Pad and its Effect on Rail Seat Deterioration (RSD)." *Proc., Trsnsportation Research Board 91st Annual Meeting*, Transportation Research Board, Washington, D.C. 20001.

Lutch, R. H., Harris, D. K., and Ahlborn, T. M. (2009). "Prestressed Concrete Ties in North America." *Proc., AREMA Annual Conference and Exposition*, AREMA, Lanham, MD 20706.

Mitchell, D. W., and Marzouk, H. (2007). "Bond Characteristics of High-strength Lightweight Concrete." *ACI Structural Journal*, 104(1), 22-29.

Murphy, R. L. (2012). "Determining the Transfer Length in Prestressed Concrete Railroad Ties Produced in the United States." Kansas State University.

Scheffe, H. (1999). The analysis of variance (Vol. 72). John Wiley & Sons.

Stachowiak, G., and Batchelor, A. W. (2013). *Engineering Tribology*, Elsevier Science.

Venables, W. N., Smith, D. M., & R Development Core Team. (2002). An introduction to R.

Walpole, R. E., Myers, R. H., Myers, S. L., & Ye, K. (1993). Probability and statistics for engineers and scientists (Vol. 5). New York: Macmillan.

Yamaguchi, Y. (1990). *Tribology of Plastic Materials: Their Characteristics and Applications to Sliding Components*, Elsevier Science.

Yu, H., Jeong, D., Choros, J., and Sussmann, T. (2011). "Finite Element Modeling of Prestressed Concrete Crosstie With Ballast and Subgrade Support." *Proc., ASME 2011 International Design Engineering Technical Conference & Computers and Information in Engineering Conference*, ASME, New York, NY 10016.